UNIVERSIDADE DA BEIRA INTERIOR
Ciências

Cancer gene therapy: design, development and *in vitro* evaluation of a plasmid DNA delivery system

Ana Raquel Bastos Neves

Dissertação para obtenção do Grau de Mestre em

Biotecnologia

(2º ciclo de estudos)

Orientadora: Professora Doutora Diana Rita Barata Costa

Coorientadora: Professora Doutora Ângela Maria Almeida De Sousa

Covilhã, junho de 2019

Acknowledgments

The elaboration of this theses concludes this stage of my academic journey. This work would not be possible without the support of some people.

First of all, thank the doctor professor Diana Costa and doctor professor Angela Sousa for the opportunity to join to your investigation team so I can research in a so interesting and actual scientific area. Thank you for all the support, effort and scientific information transmission during the entire year. Your criticisms and work suggestions were fundamental to growth as student and future professional.

I thank the University of Beira Interior, specially the Health Science Research Centre, for the facilities, equipment's and material available. Thanks to all researchers of this centre, namely of the Biopharmaceuticals and Biomaterials group, that contributed for a better work environment and that help me and shared with me important knowledge. A special acknowledgment to Ana Borges for their support in confocal microscopy experiments.

A big thank you to Margarida Almeida that was a grateful help at the beginning and to Tânia Albuquerque and Rúben Faria. Both of you helped me tremendously during the entire year, teaching me the techniques applied in this word.

To my laboratory and academic colleagues thank you for all the support and friendship. To my friends, Diana Pereira, Diana Gomes, Adriana Pinto, Rita Carapito, Rita Proença, Rosa Sequeira, Mariana Flor and Micaela Riscado, that become my family for last 5 years, a huge thank you because you made this year even more relaxed, funny and special.

Last but not least, thank to my family for the transmitted force during the year, for always believe in me. To my parents, Cristina Bastos and Francisco Neves, and brother, Francisco Neves, I have no words to write, they know how grateful I am for having them in my life. For all the efforts, education, dedication, love and support, thank you!

Resumo Alargado

O cancro é uma das principais causas de morbidade e mortalidade em todo o mundo. Envolve mudanças genéticas que afetam uma variedade de genes, como os oncogenes e genes supressores de tumor. Esta alteração leva a uma proliferação celular desregulada, angiogénese, invasão e formação de metástases. As abordagens tradicionais para o tratamento do cancro incluem quimioterapia, cirurgia e radiação. A quimioterapia representa a principal escolha de tratamento na maioria dos casos, no entanto, as terapias tradicionais são ineficazes no combate de metástases, na recorrência do tumor e no tratamento do cancro num estado mais avançado. Em alguns casos estes tratamentos são ineficazes, inespecíficos, podem danificar células saudáveis, causar resistência a fármacos e serem acompanhados por efeitos secundários indesejáveis. Portanto, novas estratégias precisam de ser desenvolvidas de forma a aumentar a eficácia terapêutica.

A terapia genética proporciona uma abordagem promissora e única à medicina devido à sua ampla aplicação no tratamento de várias doenças, incluindo doenças hereditárias e patologias adquiridas (infeção ou cancro). É uma técnica que usa ácidos nucleicos exógenos (DNA ou RNA) para reparar, substituir ou regular genes que expressem uma proteína terapêutica de interesse de forma a prevenir ou tratar uma doença. O gene supressor de tumor da proteína p53 é responsável por manter a integridade do genoma sobre situações de stress e está envolvido em várias vias celulares como a reparação do DNA, regulação do ciclo celular e indução da apoptose. No entanto, este gene encontra-se mutado ou inexistente em mais de 50 % dos cancros humanos, e, portanto, é fundamental criar protocolos de terapia génica que permitam restaurar o nível e função desta proteína. Para a terapia génica ser viável num cenário clínico é necessário desenvolver um sistema de entrega de genes eficiente. A conceção de sistemas de entrega baseados em péptidos capazes de penetrar nas células é vantajosa e pode contribuir para a evolução da terapia do cancro. Neste contexto, foi desenvolvido um novo sistema de entrega de DNA plasmídico (pDNA) codificante para a p53 com base no péptido RALA de modo a obter um sistema de entrega intracelular adequado e capaz de entregar o gene e restabelecer os níveis de p53 nas células cancerígenas.

O péptido RALA é um péptido anfipático composto por 30 aminoácidos, com uma estrutura em hélice-α que possui baixa citotoxicidade. Este péptido quando conjugado com ácidos nucleicos estabelece interações eletrostáticas e forma partículas com tamanho nanométrico adequadas para a captação celular e internalização nuclear. No presente trabalho, estes transportadores foram, numa fase inicial, caracterizados em termos de morfologia, tamanho, carga superficial e eficiência de encapsulação por microscopia eletrónica de varrimento (SEM) e através da Dispersão da Luz Dinâmica (DLS) usando o Zetasizer Nano Zs., respetivamente, e a sua estrutura analisada através de espectroscopia de infravermelho transformada por Fourier (FTIR). Os resultados mostraram que as nanopartículas formadas possuem uma forma esférica/oval, um tamanho adequado, carga global positiva e eficiências de encapsulação do plasmídeo elevadas o que indica que são

adequadas para a captação celular, internalização e libertação de genes. Além disso, estudos de estabilidade demonstraram que o péptido RALA é capaz de proteger o pDNA encapsulado das nucleases séricas e o ensaio de brometo de [3-(4,5-dimetiltiazol-2yl) -2,5-difenil tetrazolium (MTT) mostrou que estes sistemas são biocompatíveis. Experiências de microscopia confocal e de *live cell imaging* confirmaram a localização intracelular de nanopartículas e a co-localização do plasmídeo no núcleo, logo após 2 h de transfecção. Além disso, a transfecção *in* vitro de células HeLa mediada pelos vetores RALA/pDNA permitiu a deteção de transcritos de mRNA por reação em cadeia da polimerase via transcriptase reversa (RT-PCR) e expressão da proteína p53 por western blot. Um kit de ensaio de imunoabsorsão enzimático (ELISA) permitiu quantificar os níveis de proteína produzidos. A partir destes progressos, a indução de apoptose pelos sistemas RALA/pDNA nestas células cancerígenas do colo do útero foi avaliada. A ativação da caspase-3 foi monitorizada por meio de um ensaio colorimétrico e o ensaio de deteção de células em apoptose por TUNEL permitiu confirmar a fragmentação do DNA nuclear após transfecção com os poliplexos. Por último, um ensaio de western blot para marcação da proteína BAX permitiu perceber que a morte celular observada nas células tumorais transfetadas pelos nanos sistemas RALA/pDNA foi induzida pela via de apoptose intrínseca mediada pela BAX que por sua vez foi ativada pela suplementação do nível do supressor de tumor p53 nestas células. Em suma, o conjunto de resultados apresentados no presente trabalho revelam que o vetor RALA/pDNA parece ser adequado para aplicação na terapia génica do cancro.

Palavras-chave

DNA plasmídico codificante para a p53; nanopartículas; péptido RALA; proteína p53; terapia génica do cancro.

Abstract

Cancer is one of the major causes of morbidity and mortality worldwide. It involves genetic changes that affect a variety of genes, namely tumour suppressor genes. The traditional approaches for cancer treatment include chemotherapy, surgery and radiation. Chemotherapy represents the main choice of treatment in most cases, however, traditional therapies seemed unvalued to fight against metastasis, recurrence of tumour, and the treatment of advanced cancer. Therefore, new strategies need to be developed to increase therapy efficacy.

Gene therapy has brought a promising and unique approach to medicine because of its wide application in the treatment of various diseases, including hereditary diseases to acquired (infection or cancer) pathologies. p53 suppressor gene mutation or degradation is found in more than 50% of human cancers, therefore, gene therapy protocols focussed on the restauration of p53 protein are a priority in this field. For gene therapy viability in a clinical setting, the development of an efficient gene delivery system is imperative. The conception of delivery systems based on cell penetrating peptides represents an incredible asset and may deeply contribute for the evolution of cancer therapy. In this context, a new system for p53 encoding plasmid DNA (pDNA) delivery based on RALA peptide was designed and developed in order to produce a suitable intracellular delivery platform capable of gene delivery and restoration of p53 levels within the cancer cells. These carriers were characterized in terms of morphology, size, surface charge, loading and encapsulation efficiency and the fine structure was analyzed by Fourier-transformed infrared (FTIR) spectroscopy. The results showed that formed nanoparticles are suitable for cell uptake, internalization and gene release. Furthermore, stability studies demonstrated that RALA is capable of protect encapsulated DNA from serum nucleases and MTT assay showed that these systems are biocompatible. Confocal microscopy and live cell imaging experiments confirmed intracellular localization of nanoparticles, resulting in enhanced sustained pDNA uptake. Moreover, *in vitro* transfection of HeLa cells mediated by RALA/pDNA vectors allowed the detection of mRNA transcripts by RT-PCR and p53 protein expression by Western Blot. An ELISA kit assay quantified the produced protein levels. From these progresses, apoptosis in cancer cells was investigated. Caspase 3 activation was monitored by means of colorimetric assay and TUNEL assay enabled to confirm nuclear DNA fragmentation post transfection with the carriers. Lastly, a western blot assay with BAX antibody permitted to figure out which apoptosis pathway is responsible for cancer cells death. Taken together, the presented results revealed that the RALA/pDNA vector seems to be suitable as an innovative platform for p53 mediated cancer gene therapy.

Keywords

Cancer gene therapy; nanoparticles; p53 encoding plasmid DNA; p53 protein; RALA peptide.

Table of Contents

Chapter I – Introduction 1
1.1. Cancer 1
1.2. Cell apoptosis 1
1.2.1. Extrinsic and intrinsic pathways 2
1.3. Cervical cancer 3
1.4. Human Papillomavirus (HPV) 3
1.5. Prevention and risks 5
1.6. Actual therapies 5
1.7. Gene Therapy 6
1.7.1. Approaches of cancer gene therapy 7
1.7.1.1. Viral vectors 8
1.7.1.2. Non-viral vectors 9
1.7.1.2.1. Plasmid DNA 9
1.7.2. Delivery systems 12
1.8. Delivery vehicle types 12
1.8.1. Cellular barriers 15
1.9. Cell penetrating peptides 15
1.9.1 GALA and KALA peptides 16
1.9.2. RALA peptide 17
Chapter II - Aim of the thesis 19
Chapter III - Materials and Methods 21
3.1. Materials 21
3.1.1. Plasmid DNA 21
3.2. Methods 22
3.2.1. Bacterial growth conditions and plasmid production 22
3.2.2. Plasmid extraction and purification 22
3.2.3. Preparation of RALA/pDNA complexes 23
3.2.4. Determination of encapsulation efficiency (EE) 23
3.2.5. Scanning Electron Microscopy (SEM) 24
3.2.6. Particle size and zeta potential measurements 24
3.2.7. Fourier-Transformed Infrared Spectroscopy (FTIR) analysis 24
3.2.8. Circular Dichroism (CD) 25
3.2.9. Plasmid DNA protection studies 25
3.2.10. Cell culture 25
3.2.11. Cytotoxicity analysis 25
3.2.12. *In vitro* transfection studies 26
3.2.12.1. Plasmid labelling with FITC 26
3.2.12.2. Fluorescence confocal microscopy 26
3.2.12.3. Live Cell Imaging 27
3.2.13. Gene transcription 27

3.2.13.1. RNA extraction 27
3.2.13.2. cDNA synthesis 28
3.2.13.3. Reverse transcription polymerase chain reaction (RT-PCR) 28
3.2.14. Western Blot 28
3.2.14.1. Protein extraction 28
3.2.14.2. Protein quantification 29
3.2.14.3. Polyacrylamide gel electrophoresis 29
3.2.14.4. Electroblotting 29
3.2.15. Protein quantification 30
3.2.16. Caspase-3 activity 30
3.2.17. TUNEL assay 30
Chapter IV - Results and discussion 33
4.1. The properties of RALA/p53 complexes 33
4.2. pDNA protection studies 38
4.3. Cytotoxicity analysis 41
4.4. Cellular uptake and intracellular location of complexes 43
4.5. p53 gene and protein expression 50
4.6. Vector-mediated apoptosis 52
4.6.1. Caspase-3 activity assay 52
4.6.2. HeLa cells - MTT assay 53
4.6.3. TUNEL assay 53
Chapter V - Conclusions and future perspectives 57
Chapter VI - Bibliography 59
Chapter VII – Annexes 63

List of figures

Figure 1: Apoptosis intrinsic and extrinsic pathways. (Adapted from Bio Rad and Cell Signalling). 2

Figure 2: Structure of papilloma virus capsid from cryoelectron microscopy. (Protein Data Bank, May 2018) 3

Figure 3: The lifecycle of a typical hr-HPV. (Chabeda *et al*. 2018).....4

Figure 4: HPV E6 and E7 early proteins action. 5

Figure 5: Current gene therapy strategies. 7

Figure 6: Viral vectors examples used to deliver nucleic acids for gene therapy. (Adapted from (Caffery, Lee, and Alexander-Bryant 2019) 9

Figure 7: Schematic representation of a plasmid vector. 10

Figure 8: Schematic representation of the biotechnological approach used in the plasmid DNA production. 11

Figure 9: Some delivery vehicles types. (Adapted from (Lembo and Cavalli 2010)) 13

Figure 10: Barriers to intracellular trafficking of gene delivery systems. (Adapted from (Teo *et al*. 2016)) 15

Figure 11: RALA primary and secondary structure. (Adapted from (Udhayakumar *et al*. 2017)).. 17

Figure 12: Plasmid pcDNA3-FLAG-p53. (Adapted from Addgene) 22

Figure 13: Calibration curve obtained with protein standards (25-2000 µg/mL). 29

Figure 14: RALA/pDNA complexation behaviour at various N/P ratios investigated by agarose gel electrophoresis. 33

Figure 15: FTIR spectra (Transmittance (%) versus Wavenumber (cm^{-1})) of pDNA (A), RALA (B), and RALA/pDNA nanoparticles formulated at N/P ratio of 10 (C). 34

Figure 16: Representation of circular dichroism spectra of RALA peptide (40 µM) (A) and RALA/pDNA vectors at N/P ratio of 2, 5 and 10 (B). 35

Figure 17: Scanning electron micrographs of RALA/p53 nanoparticles formulated at N/P ratios of 1, 2, 5, 10, 15, 20 and 50. 36

Figure 18: Electrophoretic analysis of the vector's protection of pDNA after its incubation with serum supplemented DMEM + 10 % FBS. 38

Figure 19: Electrophoretic analysis of the vector's protection of pDNA after its incubation with DNase I and DNase I + 10 % SDS for 1 h. 39

Figure 20: Electrophoretic analysis of the vector's protection of pDNA after its incubation with trypsin. 40

Figure 21: Electrophoretic analysis of the vector's protection of pDNA after its incubation with 10 % FBS. 41

Figure 22: Cellular viability of fibroblast cells after 24 h or 48 h of transfection with RALA/pDNA nanoparticles at various N/P ratios. 42

Figure 23: RALA/pDNA vectors transfection ability and intracellular co-localization investigated by fluorescence confocal microscopy after 2 h of transfection. 44

Figure 24: RALA/pDNA vectors transfection ability and intracellular co-localization investigated by fluorescence confocal microscopy after 4 h of transfection. 44

Figure 25: RALA/pDNA vectors transfection ability and intracellular co-localization investigated by fluorescence confocal microscopy after 6 h of transfection. 45

Figure 26: Representative live cell images of the transfection mediated by RALA/pDNA nanoparticles at N/P ratio of 2..... 47

Figure 27: Representative live cell images of the transfection mediated by RALA/pDNA nanoparticles at N/P ratio of 5..... 48

Figure 28: Representative live cell images of the transfection mediated by RALA/pDNA nanoparticles at N/P ratio of 10. 49

Figure 29: PCR analysis of p53 mRNA in HeLa cells after 24 h of transfection mediated by RALA/pDNA nanoparticles prepared at N/P ratios of 2, 5 and 10. 50

Figure 30: Evaluation of p53 and BAX protein expression by western blot analysis after 48 h transfection with RALA/pDNA nanoparticles prepared at N/P ratios of 2, 5 and 10. 51

Figure 31: Caspase-3 activity in HeLa cells after 48 h of transfection mediated by RALA/pDNA vectors at N/P ratios of 2, 5 and 10. 52

Figure 32: Cell viability of HeLa cells after 24 and 48 h of transfection with RALA/pDNA complexes at different N/P ratios. 53

Figure 33: In situ cell death detection in HeLa cells assayed by terminal deoxynucleotidyl transferase-mediated dUTP nick end labelling (TUNEL). 54

Figure 34: Abstract submitted to XIV Annual CICS-UBI Symposium. 63

Figure 35: Scientific article submission proof email..... 64

List of Tables

Table 1: Example of practical applications of carriers in gene therapy. 14

Table 2: Examples of other studies using RALA peptide as carrier. 18

Table 3: Mean size, polydispersity index, average zeta potential and pDNA encapsulation efficiency (EE) for RALA/pDNA complexes formulated at several N/P ratios. 37

Table 4: Quantification of p53 protein levels in HeLa cells after 24 h of transfection mediated by the formulated RALA/pDNA systems formulated at N/P ratios of 2, 5 and 10. 51

List of Abbreviations

µg: Microgram
µm: Micro millimetre
µM: Micro molar
3D: Three-dimensional
A: Ampere
BAK: Bcl-2-antagonist killer
Bax: Bcl-2-associated X protein
Bcl-2: B-cell lymphoma 2
BSA: Bovine serum albumin
CD: Circular Dichroism
cDNA: Complementary Deoxyribonucleic acid
CICS: Health Sciences Research Centre
cm: Centimetre
CO_2: Carbon Dioxide
CpG: Cytosine-phosphate-guanine
CPP: Cell Penetrating Peptides
DAPI: 4',6-diamino-2-fenillindol
DEPC: Diethylpyrocarbonate
DLS: Dynamic Light Scattering
DMEM-HG: Dulbecco´s Modified Eagle Medium, high glucose
DNA: Deoxyribonucleic acid
dUTP: Deoxyuridine Triphosphate
E. coli: *Escherichia coli*
e.g.: for example
ECL: Enhanced Chemiluminescence
EDTA: Ethylenediamine tetraacetic acid
EE: Encapsulation Efficiency
EGTA: Ethylene Glycol Tetraacetic Acid
ELISA: Enzyme-Linked Immunosorbent Assay
EMA: European Medicines Agency
etc.: et cetra
EU: Endotoxin Unit
FBS: Fetal bovine serum
FDA: Food and Drug Administration
FITC: Fluorescein Isothiocyanate
FMOC: Fluorenylmethyloxycarbonyl
FTIR: Fourier-transform infrared spectroscopy
g: G Force

g: Grass
gDNA: Genomic DNA
h: Hour
HCl: Hydrochloric acid
He-Ne: Helium-Neon
HEPES: 4-(2-hydroxyethyl)-1-piperazineethanesulfonic acid
HPV: Human Papillomavirus
hr: high risk
IgG: Immunoglobulin G
K_2HPO_4: Potassium hydrogen phosphate
kb: kilobase
kbp: Kilo base pair
kDa: Kilo Dalton
KH_2PO_4: Potassium dihydrogen phosphate
kV: Kilovolt
L: Litter
LB: Luria-Bertani
M: Molar
$MgCl_2$: Magnesium chloride
min: Minute
mL: Millilitre
mm: Millimetre
mM: Millimolar
MM: Molar Mass
MOPS: 3-(N-morpholino)propanesulfonic acid
mPa: Megapascal
mRNA: Messenger RNA
MSNs: Mesoporous silica nanoparticles
MTT: 3-(4,5-Dimethylthiazol-2-yl)-2,5-Diphenyltetrazolium Bromide
mV: Millivolts
Mw: Molecular weight
N: Amine groups
N: Normality
NaCl: Sodium chloride
NaOH: Sodium hydroxide
ng: Nanogram
NHDF: Normal Human Dermal Fibroblasts
NIBS: Non-Invasive Backscatter Optics
nm: Nanometer
nm: nanometre

O_2: Oxygen
ºC: Degree Celsius
oc: open circular
OD: Optic Density
OH: Hydroxyl
Ori: origin of replication
P.I.: Polydispersive index
P: Phosphate groups
PAGE: Polyacrylamide gel
PALS: Phase Analysis Light Scattering
PBS: Phosphate buffer solution
pcDNA: Plasmid cloning DNA
pDNA: Plasmid DNA
PFA: Paraformaldehyde
PMSF: Phenylmethylsulfonyl fluoride
pNA: p-Nitroaniline
pRb: retinoblastoma protein
PVDF: Polyvinylidene difluoride
RNA: Ribonucleic acid
rpm: Revolutions per minute
RT-PCR: Reverse transcription polymerase chain reaction
s: Second
sc: super coiled
SDS: Sodium dodecil sulphate
SEM: Scanning electron microscope
siRNA: Silencing RNA
spp.: species
ST: Standard deviation
TAE: Tris-acetate-EDTA
TB: Terrific Broth
TdT: Terminal deoxynucleotidyl transferase
TUNEL: Terminal deoxynucleotidyl transferase dUTP nick end labeling
UBI: University of Beira Interior
UV: Ultraviolet
v/v %: Volume per volume percentage
V: Voltage
Vis: Visible
VLPs: Virus like particles
w/v %: Weight per volume percentage

List of Scientific Communications

Oral presentation

Bastos, A.; Sousa, A; Faria, R.; Albuquerque, T.; Queiroz, J; Costa, D. Cancer gene therapy: design, development and *in vitro* evaluation of a RALA peptide/pDNA vector. XIV Anual CICS-UBI Symposium. 4-5 July 2019, Covilhã, Portugal.

List of Scientific Publications

A. R. Neves, A. Sousa, R. Faria, T. Albuquerque, J. A. Queiroz, D. Costa. 2019. Cancer gene therapy mediated by RALA/plasmid DNA vectors: Nitrogen to Phosphate groups ratio (N/P) as a tool for tunable transfection efficiency and apoptosis. *ACS Applied Materials & Interfaces* (Submitted).

Chapter I – Introduction

1.1. Cancer

Cancer is one of the major causes of morbidity and mortality worldwide. (El-Deeb *et al*. 2018) The knowhow of cancer biology has grown tremendously, and it is now widely understood to originate from genetic instability as well as microenvironment factors. (Teo *et al*. 2016) It involves genetic changes that affect oncogenes, tumour suppressor genes and modifier genes, which enable them to sustain proliferative signalling, evade growth suppressors, resist cell death, induce angiogenesis, enable replicative immortality and activate invasion and metastasis.(Costa *et al*. 2014; Teo *et al*. 2016)

The tumour suppressor gene p53 keeps the genome integrity under oncogenic stress or other stress signals and it is involved in several cellular pathways such as DNA repair, regulation of the cell cycle and induced apoptosis (programmed cell death). At the molecular level, mutation of the p53 gene is found in greater than 50 % of human tumours. Mutations in p53 abrogate normal tumour suppressor functions, contributing to the survival and/or proliferation of abnormal cells with poorly differentiated phenotypes. Cancer cells containing mutant p53 are associated with more aggressive disease, increased resistance to chemotherapy and radiation therapy, and poor prognosis. In this sense, restoration of p53 functions in tumour cells could result in tumour inhibition, normal cell division and adequately responses to DNA damaging and to impede angiogenesis. (Guidotti, Brambilla, and Rossi 2017; Sharma *et al*. 2011; Costa *et al*. 2014)

1.2. Cell apoptosis

In apoptosis, internal and/or external stimuli initiate a series of highly controlled reactions, which ultimately lead to cell death. The two most important groups of proteins involved in apoptosis, caspases and the Bcl-2 (B-cell lymphoma 2) family of proteins, participate in all pathways of apoptotic cell death. (Grilo and Mantalaris 2019)

Caspases are cysteine-dependent endoproteases that catalyse the breaking of the peptide bond. Most caspases can be classified, according to their role, in initiator caspases, executioner caspases and caspases involved in inflammation. Caspase-2 shares structural elements with both initiator and executioner caspases. (Grilo and Mantalaris 2019)

Proteins of the Bcl-2 family are heavily involved in the regulation of apoptosis both with pro- and anti-apoptotic activities. (Grilo and Mantalaris 2019)

1.2.1. Extrinsic and intrinsic pathways

The extrinsic pathway is triggered by stimuli external to the cells, designed death ligands. (Figure 1) (Grilo and Mantalaris 2019) These death ligands bind to a death receptor family member with a broad of cell death and survival, differentiation or immune regulation. (Fulda and Debatin 2006; Venere *et al*. 2018) Once signal transduction have begun externally, cytoplasmic adaptor proteins are recruited to the intracellular domain of the receptors and serve to bind and aggregate procaspase-8 to create a death-inducing signalling complex (DISC) that serve to activate downstream effector caspases, caspase 3 and/or 7, and induce apoptosis. (Venere *et al*. 2018)

As depicted in Figure 1, the intrinsic pathway is activated by internal stimuli by the mitochondria in recognition of cellular stress. (Venere *et al*. 2018) These stimuli promote the activation of caspases and pro-apoptotic members of the Bcl-2 family leading to mitochondria outer membrane permeabilization via BAX (Bcl-2-associated X protein) channels. (Grilo and Mantalaris 2019)

The tumour suppressor p53 is an example of protein that can directly trigger permeabilization of the outer mitochondrial membrane via BAX activation. Upon disruption of the outer mitochondrial membrane, a set of proteins normally found in the space between the inner and outer mitochondrial membranes is released, including cytochrome c. The release of cytochrome c directly triggers caspase-3 activation. Then, caspase-3 cleaves key substrates in the cell to produce many of the cellular and biochemical events of apoptosis. (Fulda and Debatin 2006)

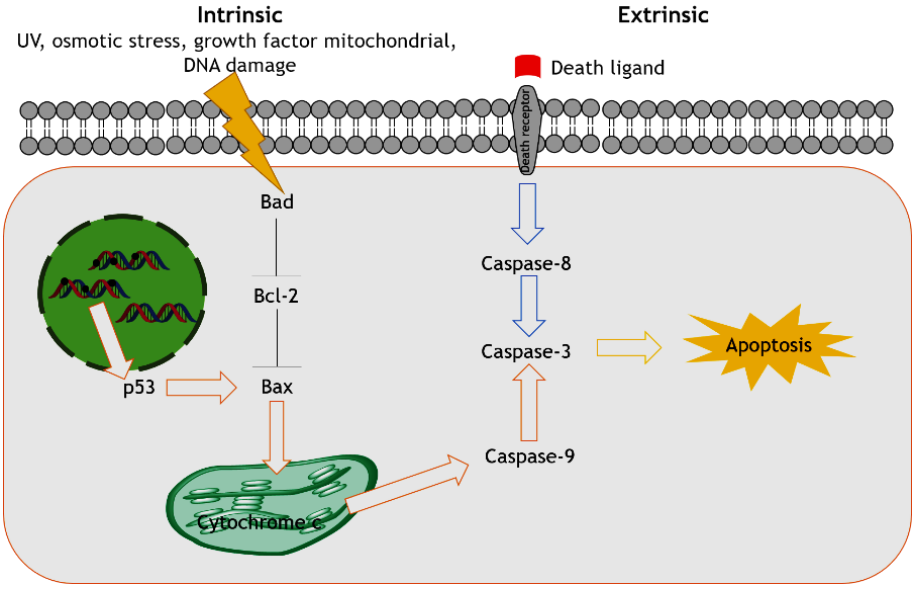

Figure 1: Apoptosis intrinsic and extrinsic pathways. (Adapted from Bio Rad and Cell Signalling).

1.3. Cervical cancer

It is estimated that Human papillomavirus (HPV) related cancers account for 5% of all human cancers. Cervical cancer is an important disease, more so than other cancers (breast, colorectal) as it affects women below the age of 45 and it is the second most common cancer in women. (Ali *et al*. 2017) This cancer originates in cervix region, the narrow portion of the uterus where it joins with the top of the vagina. Most cervical cancers are squamous cell carcinomas, arising in the squamous epithelial cells that line the cervix. (Medina-Alarcon *et al*. 2017)

HPV is the most common cause of cervical cancer and the 4th most common cancer in women worldwide. (Chabeda *et al*. 2018) In low- and middle-income countries is the second most common cancer and is responsible for approximately 85 % of total new cases worldwide. Most recent data suggest that 90 % of cervical cancer deaths occurred in these countries. As a global health priority, cervical cancer control serves as an example of the substantial differences between countries regarding public health priority, healthcare resources and infrastructure, cultural barriers, technology, and ability to address prevention and treatment strategies. (Vu *et al*. 2018)

In 2017, cancer was the second most frequent cause of death in women. 0.4 % of this malignant tumour's cases were caused by HPV virus. (Direção-Geral Saúde, Instituto Nacional de Estatística, Causas de morte - 2017)

1.4. Human Papillomavirus (HPV)

Human papillomavirus are small non-enveloped double-stranded DNA viruses with a genome size of approximately 8 kb. The capsid is 50–60 nm in diameter and is arranged in a quasi-icosahedral formation (Figure 2). (Chabeda *et al*. 2018)

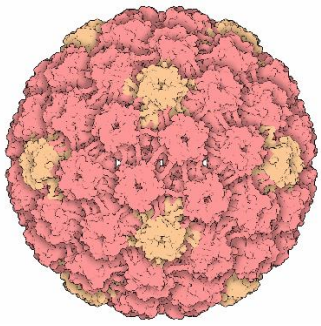

Figure 2: Structure of papilloma virus capsid from cryoelectron microscopy. (Protein Data Bank, May 2018)

There are at least 170 HPV genotypes described, which are categorised into two groups: the low-risk types which cause genital, common and flats warts, verruca's or myrmecia as well as many other skin lesions, and high risk HPV (hr-HPV) types which are responsible for 99.7 % of cervical cancer cases. HPV-16 and -18 are the most prevalent types, causing more than 70 % of cases. (Chabeda *et al*. 2018)

HPV infects basal epithelial cells through anatomically accessible points such as microlesions in the skin, genital organs and oropharyngeal areas. Most infections are cleared by the immune system; however, some benign cervical lesions can progress to cancer. When the viral genome integrates into the host genome and replicate until it reaches a huge number of copies (Figure 3). (Chabeda *et al*. 2018; Ali *et al*. 2017)

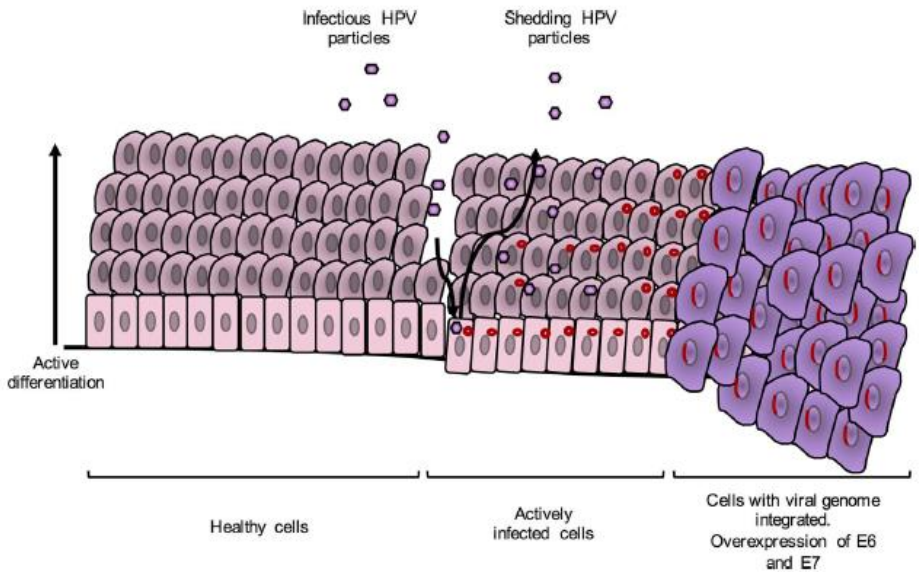

Figure 3: The lifecycle of a typical hr-HPV. (Chabeda *et al*. 2018)

HPV infection process starts when capsid proteins L1 and L2 attach to epithelial cell receptors and a long process of entry commences, resulting in cytoplasmic uncoating of the virus and entry of its genome into the nucleus of the infected cell, where it is transcribed and then replicated. The early proteins are expressed first and regulate the host cell life cycle and genome replication (Figure 4). The E6 protein promotes the degradation of the host apoptosis regulator protein p53 via cellular ubiquitination and activates telomerase resulting in disruption of the control of cell cycle progression and extended cell life. The E7 protein targets and disturbs the tumour suppressor retinoblastoma protein (pRb) by repressing regulation of replication-associated genes and leading to the transition of the cell life cycle to the S-phase and subsequent host cell genome replication. E6 and E7 disrupt the cell cycle regulation and promote prolonged host cell life, leading to genomic instability. Maturation of virions occurs after terminal differentiation of epithelial cells, and their release coincides with natural

shedding of senescent cells at the end of the epithelial cell life cycle. (Chabeda *et al*. 2018; Ali *et al*. 2017)

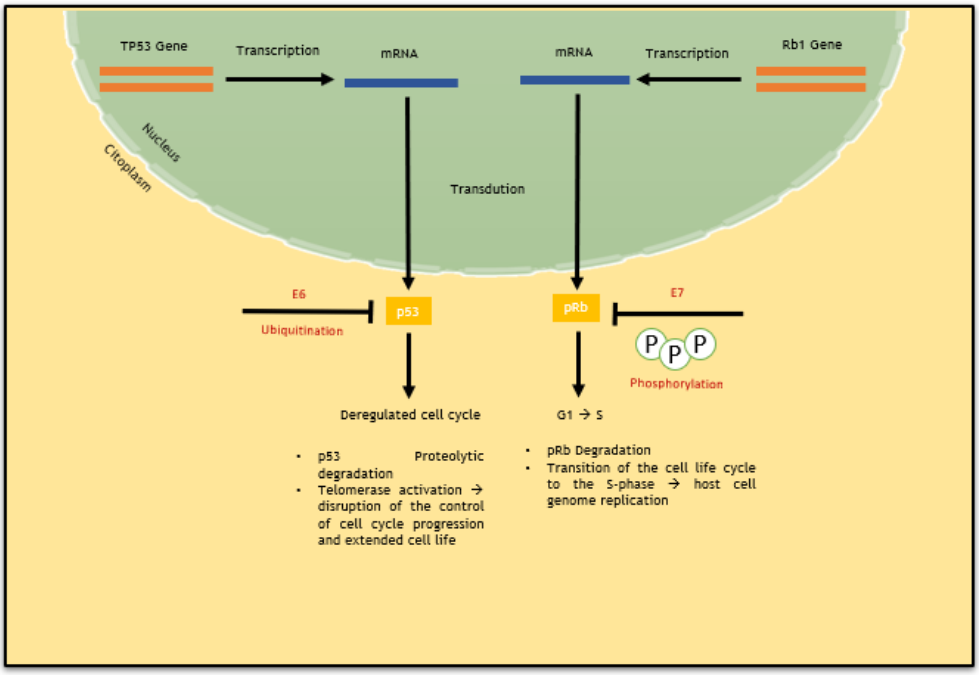

Figure 4: HPV E6 and E7 early proteins action.

1.5. Prevention and risks

Testing with a "Pap smear," more technically referred to as cytology, has been the most pervasive and effective primary screening method used in high-resource settings. (Rizzo and Feldman 2018)

Not all HPV infections confer the same risk of malignancy. Many factors, behind (epi)genetic changes within the cell, can affect the risk of developing cervical cancer, including host and environmental factors which allow a patient to clear the viral infection, such as age, immunocompetence, or tobacco use, as well as the oncogenic potential of different HPV types. (Rizzo and Feldman 2018) The microbiome at individual body sites can have profound effects on cancer development too. Interestingly, changes in the cervicovaginal microbiome occur during progression from HPV-positive lesions to cervical cancer, which include an increased diversity of resident bacteria and a reduction in *Lactobacillus* spp. (Hoppe-Seyler *et al*. 2018)

1.6. Actual therapies

Currently, there are three commercially available prophylactic HPV vaccines on the market: Cervarix®, a bivalent HPV-16/18 vaccine; Gardasil®, a tetravalent HPV-6/11/16/18 vaccine; and Gardasil®9, a nonvalent HPV-6/11/16/18/31/33/45/52/58 vaccine. All exploit the fact that HPV

L1 protein can form virus-like particles (VLPs) when expressed alone in a variety of cell types, that are morphologically and antigenically highly similar to native virions. These three vaccines effectively prevent HPV infections caused by the targeted types by eliciting the production of neutralising antibodies that bind to the viral particles and block their entrance into host cells. However, these vaccines are not effective at eliminating pre-existing infections, since the target antigens, L1 capsid proteins, are not expressed in infected basal epithelial cells. Therefore, individuals already infected with HPV do not benefit from the current vaccines. (Chabeda *et al*. 2018)

There are strong efforts to develop next-generation vaccines based on the viral L2 minor structural protein, which are expected to protect against a broader range of HPV types. However, there are still important issues to be resolved. Firstly, widespread application of vaccines in less-developed-countries is substantially hindered by financial and logistic hurdles. Indeed, only a small minority (7.5 %) of females worldwide, aged 10-20 years, are estimated to have received at least one shot of an HPV vaccine. In Portugal, in Nacional Programme of Vaccination there are available only the Gardasil®9 vaccine. Complete vaccination implies the administration of two doses by intramuscular via to girls with 10 years old. (Direção-Geral de Saúde, 2018) Secondly, HPV-induced carcinogenesis results from a persistent infection with oncogenic HPV types in a process lasting several decades. Since the introduced vaccines are prophylactic, they do not eliminate persistent HPV infections or interfere with their progression to malignancy. (Hoppe-Seyler *et al*. 2018; El-Deeb *et al*. 2018)

The traditional approaches for cancer treatment include chemotherapy, surgery and radiation. Chemotherapy represents the main choice of treatment in most cases. Thus, HPV-linked carcinogenesis will remain a major health problem for the next decades and new treatment options are urgently required. (Hoppe-Seyler *et al*. 2018; El-Deeb *et al*. 2018)

1.7. Gene Therapy

Although traditional therapies can improve the curing effects in the early stage of cancer in some extent, they seem unvalued to fight against metastasis, recurrence of tumour, and the treatment of advanced cancer. (Liu *et al*. 2015) In some cases these aggressive therapies are unsuccessful, unspecific and can damage normal healthy cells, can cause multidrug resistance and they are always accompanied by inevitable side effects. (Guidotti, Brambilla, and Rossi 2017; Costa *et al*. 2014)

Gene therapy has brought a promising and unique approach to medicine because of its wide application in the treatment of various diseases, including hereditary diseases to acquired (infection or cancer) pathologies. (Wang, Dou, and Bao 2014; Costa *et al*. 2019) This technology uses, permanent or transient, exogenous nucleic acids to repair, replace or regulate genes to

express a protein of therapeutic interest and prevent or treat several diseases. (Kim *et al*. 2015; Hardee *et al*. 2017) It has been demonstrated that therapeutic nucleic acids delivered into target cells can treat various diseases including cancers and genetic diseases. (Zhang *et al*. 2017) For example, tumour suppressor genes can be upregulated, or mutated oncogenes downregulated in affected cells, as well as the delivery of suicide genes can signal cell death. (Kim *et al*. 2015)

Gene therapy can be used alone or as an adjuvant to the other mentioned therapies since certain genes can sensitize tumour cells to radiation or drugs enhancing the effect of the clinical approach. (Costa *et al*. 2014)

1.7.1. Approaches of cancer gene therapy

Gene therapy may be carried out by first removing the cells of interest from patients and subsequently reintroducing cells that have been appropriately genetically modified. Alternatively, genetic materials can be directly introduced into the target organs or tissues of the patients (Figure 5A). Different types of gene therapy, including gene augmentation, gene-specific targeting, and most recently, genome editing, have been developed over the prior few decades (Figure 5B-D). (Lee *et al*. 2019)

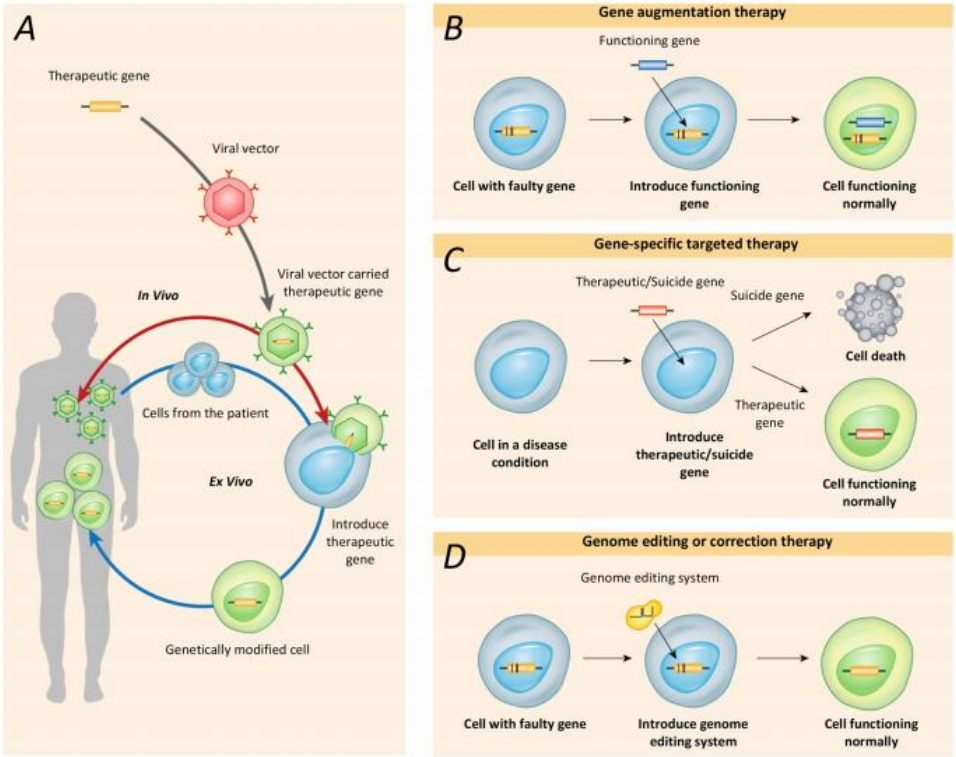

Figure 5: Current gene therapy strategies.(A) Health-related or therapeutic genes are directly introduced into the body (red line) or into cells that are removed from the body and then returned to the patient (blue line). Gene therapies utilize several mechanisms, including gene augmentation therapy, gene targeting therapy and genome editing therapy. (B) Gene augmentation therapy replaces a disease-causing

gene with a healthy copy of the gene. (C) Gene-specific targeted therapy introduces a new gene or inactivates a disease-causing gene in the body to help treat a disease. (D) Genome editing therapy modifies or corrects a disease-causing gene. (Lee *et al*. 2019)

Gene augmentation therapy refers to the introduction of a new functional gene into the host genome to compensate for a faulty gene. By adding a functional copy of the faulty gene into the genome, this approach aims to express the functional gene at sufficient levels to replace the missing or dysfunctional protein. (Lee *et al*. 2019) This gene therapy approach has been used to delivery apoptotic and tumour-associated genes to cancer cells. p53 gene is an example. This gene is delivered to cancer cells in order to restore p53 function and kill tumour cells via apoptosis, cell aging, activating immune system of the host, etc. Even at the advanced stage, restoration of damaged p53 pathway can stop tumour growth. The novel findings have suggested a greater role of p53 in clinical application of gene therapy. (Liu *et al*. 2011; Chen *et al*. 2018)

Gene-specific targeted therapy refers to the introduction of genetic materials such as DNA or RNA, designed to specifically alter inappropriate gene activity caused by diseases, or the addition of copies of a gene for protective or regenerative purposes. By manipulating genes involved in pathological changes or their related molecular pathways, gene-specific targeted therapies provide attractive therapeutic strategies for the long-term treatment of nongenetic diseases and autosomal dominant genetic diseases. (Lee *et al*. 2019)

Genome editing or correction therapy directly repairs and transforms the mutated gene into a normally functioning gene. Thus, this approach has the potential to fundamentally correct mutant genes. It is particularly attractive for the treatment of inherited diseases (autosomal dominant, autosomal recessive and X-linked diseases) caused by genes with very specific spatial and stoichiometric expression. (Lee *et al*. 2019) However, form all these approaches of cancer gene therapy it is fundamental use viral or non-viral vectors to deliver the target genetic information.

1.7.1.1. Viral vectors

Viral vectors (Figure 6) were the first delivery systems used for gene therapy. (Caffery, Lee, and Alexander-Bryant 2019) Despite the high efficacy of viral vectors such as retroviruses, adeno-associated viruses, lentiviruses and adenoviruses at integrating host genome and delivering genes, they can cause immunogenicity, nonspecific insertion and oncogene activation. Besides, their use currently involves high manufacturing costs, restrictions in the DNA size and perhaps most importantly patient perception. They could lead to the generation of neutralising antibodies which restrict repeated therapy. (Teo *et al*. 2016; Chabeda *et al*. 2018; Shao *et al*. 2017; Bennett *et al*. 2015)

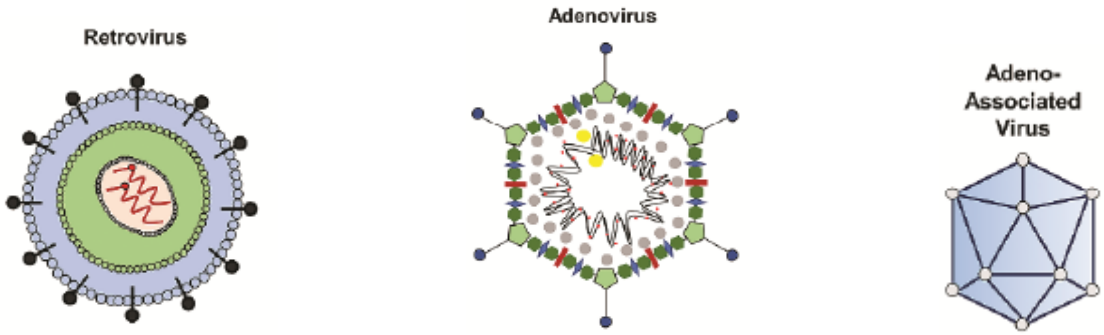

Figure 6: Viral vectors examples used to deliver nucleic acids for gene therapy. (Adapted from (Caffery, Lee, and Alexander-Bryant 2019)

1.7.1.2. Non-viral vectors

A variety of non-viral delivery systems, such as liposomes and polymers, have been tested for gene delivery and will be discussed further. Other non-viral gene delivery vectors as naked RNA or DNA molecules are biocompatible, easily manufactured and relatively inexpensive, reproductible and synthetically modular. However, their lower gene transfection efficiencies compared to viral vectors act as a hurdle to their clinical usage. So, they are usually complexed with delivery vehicles (e.g., cationic lipids, cationic polymers, etc.) or subjected to forced entry (electroporation, hydrodynamic injection, etc.). For instance, plasmid DNA has been extensively explored in this field because of its modular nature allowing for straightforward molecular cloning, making it easy to manipulate and design for therapeutic use. (Hardee *et al.* 2017)

1.7.1.2.1. Plasmid DNA

The enormous potential of plasmids as non-viral vectors in gene therapy has been recognized since at least 1990. (Hardee *et al.* 2017)

Plasmid vectors represent an important platform for gene delivery as they are safe, stable in storage, easy to manipulate and relatively inexpensive to produce. Plasmids are small circular double-stranded DNA molecules capable of self-replicating in bacterial host cells. Their size ranges from 0.8 to 200 kbp. (Pahle and Walther 2016)

Conventional plasmids contain numerous genetic elements necessary for the plasmid DNA (pDNA) production (origin of replication (Ori), antibiotic resistance genes and eukaryotic selection marker) and suitable for gene therapy (promoters, the gene of interest and terminator). (Figure 7) (Pahle and Walther 2016) The *ori* allows propagation and self-replication in a bacterial host strain and antibiotic resistance-encoding genes allows selection of plasmid-harbouring. Eukaryotic selection marker promotes plasmid stability and improved transcriptional efficacy and selectivity. Promoters plays a key role in transcription regulation

of associated genes. The presence of a strong transcriptional terminator downstream of the encoding sequence prevents transcription of vector sequences, enhances plasmid stability and provides protection against degradation. (Hardee *et al*. 2017; Singha *et al*. 2017)

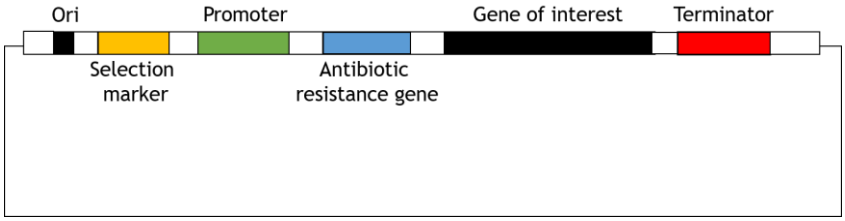

Figure 7: Schematic representation of a plasmid vector.

The pDNA has five conformations, the open-circular (oc), relaxed circular, linear, supercoiled (sc) and the supercoiled denatured conformation. Oc and linear conformations arise through single-stranded and double-stranded nicks, respectively. These plasmid forms have been deemed undesirable for clinical purposes, due to a perceived increased risk of recombination events and integration into genomic DNA (gDNA). These forms may also be subject to more rapid intracellular degradation. Sc conformation is the native pDNA isoform, presents a compact conformation and consists of complete double strand with the normal twist and shape. It is the one of choice in gene therapy due to its outstanding stability, eminent antigenicity and the more efficient for gene transfection of all isoforms. (Abdulrahman and Ghanem 2018; Valente *et al*. 2014; Ghanem, Healey, and Adly 2013)

Plasmid manufacturing can be divided into various steps (Figure 8):

1. Cell culture: after selecting a specific strain and the target plasmid, the host is cloned. This is followed by the amplification of pDNA copies, in an adequate host, by fermentation at specific and optimized growth conditions;
2. Downstream processing: the main aim of this step is to extract and isolate the pDNA in a reasonable purity that meets the pharmaceutical specifications and get rid of the other cell impurities like RNA, proteins and gDNA. The whole process consists of three stages: preliminary purification, intermediate purification and final purification. In the preliminary purification step, the high-density broth of cells harvested from fermentation step was collected by centrifugation or microfiltration. Subsequently, the cells are lysed to liberate the pDNA by alkaline lysis methods. In the second step, clarification and pre-purification procedures are taken to decrease the levels of impurities in the lysates and concentrate the pDNA lysate sample for the final purification stage;
3. Purification: this is the most important and expensive step of all biotechnology pDNA obtention process. In addition to being dependent on the efficiency of the previous production process is essential to ensure the purity recommended by regulatory agencies

in order to continue with its application and profitability of the process. Various purification procedures can be taken like precipitation, ultrafiltration and aqueous two-phase systems; nevertheless, liquid chromatography is certainly the most extensively implemented technique. The purification technique must guarantee good solution appearance (clear, colourless), at least 97 % purity of the final obtained sc pDNA, the RNA and protein content should not be detectable, the amount of gDNA needs to stay above 2 ng/µg of pDNA and the level of endotoxins should not be more than 0.1 EU/µg of pDNA. (Abdulrahman and Ghanem 2018; Valente *et al*. 2014)

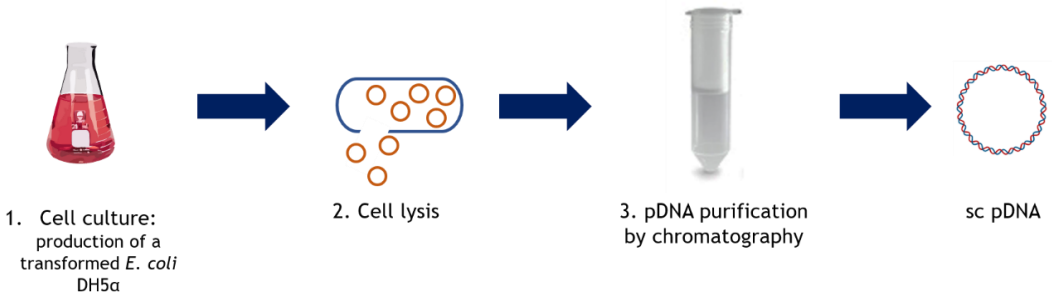

Figure 8: Schematic representation of the biotechnological approach used in the plasmid DNA production.

However, the use of plasmid vectors for gene therapy are beset with some notable inherent limitations:

- Most plasmid DNA preparations contain also the non-functional open circular and linear isoforms;
- They are non-replicating episomes, transgene expression is transient and diluted by cell division;
- Bacterial sequences in plasmids can contribute to their gene silencing;
- Unmethylated cytosine-phosphate-guanine (CpG) dinucleotides have the potential to be recognized by the mammalian immune system, potentially precipitating not only transgene silencing but also immune response;
- The bacterial origin of replication (ori) potentially allows plasmids meant to deliver therapeutic sequences to also inadvertently transfer into and replicate in other bacteria;
- Plasmids encode antibiotic resistance-encoding genes for selection of plasmid-harbouring bacteria. The use of antibiotics and their resistance genes in the preparation of plasmid vectors is discouraged by regulatory bodies such as the Food and Drug Administration (FDA) and the European Medicines Agency (EMA) because of the risk of transfer and replication of resistance genes to bacteria in the human microbiome and possibly into the environment. Residual antibiotics that remain from vector production may also trigger an immune reaction in patients.(Hardee *et al*. 2017)

- Plasmids in its native form present some instability in the presence of serum nucleases, as well as low transfection efficiency due to the repulsion by the eukaryotic membrane induced by negative charge of phosphate groups, between other, being fundamental to combine the pDNA with an adequate delivery system.

1.7.2. Delivery systems

The application of nucleic acids in gene therapy is a challenge because of its inability in the extracellular matrix and its inability to cross the eukaryotic cell membrane barrier and reach the nucleus in its native solution form. In order to minimize these limitations and maximize the pDNA transfection efficiency, various delivery system types have been investigated. The use of a suitable delivery vector can compact the nucleic acids providing stability, protection from enzymatic degradation and innate immune system, extravasation from the vasculature and efficient translocation inside the cell through attachment to the target cells, cell membrane passage, endolysosomal escape to reach the cytosol and transport to the nucleus to induce the therapeutic effect. (Jain *et al*. 2015; McCarthy *et al*. 2014; Costa *et al*. 2015) The carriers should have a suitable size (nanometer range), incorporate large amounts of DNA, be capable of release the payload in a sustained manner and must be biocompatible, elicit minimal side-effects and have good biodistribution. (Costa *et al*. 2015)

While physical methods of delivery enhancement, such as using ultrasound, heat, light, and applied magnetics or electric fields, have been utilized to deliver gene carriers to target cancer sites, these methods rely on precise knowledge of the location of tumours. To reach both known and unknown locations of cancer cells, other research efforts have focused on the development of viral and non-viral vectors that can be combined to obtain the ideal delivery vehicle to ensure site-specific accumulation and cancer-specific transfection through both passive and active targeting. (Kim *et al*. 2015)

1.8. Delivery vehicle types

Delivery vehicles are engineered so that they are attracted specifically to diseased cells, which allows the target delivery of drugs, proteins or nucleic acids for the direct treatment of those cells, improving efficacy, decreasing side effects and overall improving human health. (Jahangirian *et al*. 2017)

Cationic lipid-based vectors (liposomes) (Figure 9) are safe, cost-effective, easier to fabricate and have a great potential for solubilizing, encapsulating and administering drugs with a potential to improve drug absorption thereby contributing with their bioavailability and minimizing side effects. For synthesis of these nanocarriers the most materials are biocompatible lipids. One of the biggest problems of their use includes the high toxicity at low

specificity and sensitivity to serum components. (Medina-Alarcon *et al*. 2017; Martinez-Negro *et al*. 2018; Teo *et al*. 2016; Pahle and Walther 2016)

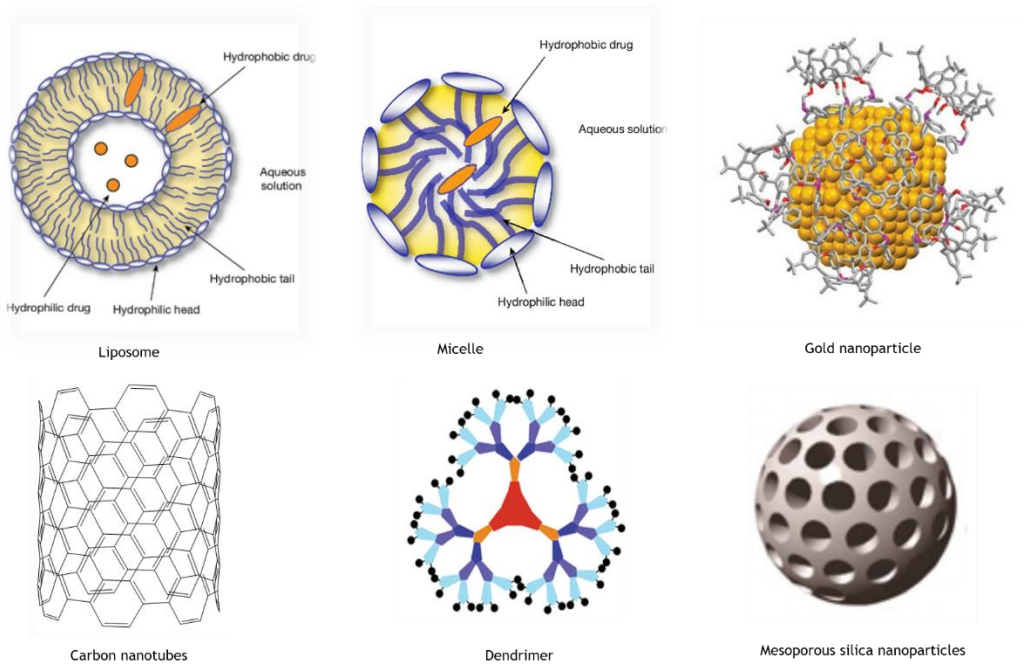

Figure 9: Some delivery vehicles types. (Adapted from (Lembo and Cavalli 2010))

Polymeric nanoparticles are high tailorable, durable, easy to prepare, purify and chemically modify, are stable and protect against enzymatic degradation, allows controlled release, prolonged circulation half-life and high penetration capacity. However, there are some disadvantages as the degradation and high cost to manufacture. (Medina-Alarcon *et al*. 2017; Teo *et al*. 2016)

Metallic or inorganic nanoparticles (Figure 9) are used for distribution of targeted drugs, gene delivery and in the diagnosis. Gold nanoparticles due to their favourable physical, chemical and photometric properties are frequently applied in cancer therapy as drug transporters or with other drugs for penetrating tumour cells, thus decreasing the dose of the drug and improving the response to tumour cells. Another very encouraging class of nanoparticles is the multi-walled carbon nanotubes (Figure 9) and magnetic nanoparticles as they carry plasmids which can target tumours. The major drawback by using inorganic particles is their slow biological clearance and unwanted persistence. (Medina-Alarcon *et al*. 2017; Pahle and Walther 2016)

Dendrimers (Figure 9) are highly branched 3D polymers. They are capable of penetrate cellular and endosomal membranes. (Caffery, Lee, and Alexander-Bryant 2019) Can incorporate small molecules by electrostatic or hydrophobic interactions, and the drugs can be bonded on their

surface through polar interchanges. Are used in medical and biotechnological applications due to their biocompatibility. (Medina-Alarcon *et al*. 2017)

Micelles (Figure 9) are amphiphilic copolymers that have a hydrophobic core/hydrophilic shell structure. (Caffery, Lee, and Alexander-Bryant 2019) Micelles allow a great depth of tissue penetration for targeted drug delivery and they usually disintegrate rapidly in the body. Despite the capability to load drug and gene, micellar systems need to display high thermodynamic and kinetic stability to prevent premature drug release when administered in the blood stream. (Medina-Alarcon *et al*. 2017; Teo *et al*. 2016)

Mesoporous silica nanoparticles (MSNs) have been used to deliver small molecules, genes, and proteins. Their large surface area provides space and binding sites to accommodate nucleic acids via non-covalent encapsulation or direct covalent conjugation. Their pores allow the accommodation of small molecules and their surface can be engineered with cationic polymers to encapsulate nucleic acids via electrostatic binding. (Jiang *et al*. 2016)

Several nanocarriers have been developed and applied *in vitro*, some of which are described herein (Table 1).

Table 1: Example of practical applications of carriers in gene therapy.

Nanocarrier	**Nanocarrier composition**	**Pharmacist**	**Genetic agent**	**Cell line**	**References**
Liposomes	Cholesterol-DSPC-DDAB-DSPE-PEG2000	---	pDNA	H1299 and NCI-H69 cells	Gjetting *et al*. 2011
Polymeric	PEI-MTX	---	pDNA	Cervical cancer HeLa cells	Costa *et al*. 2018
Inorganic	Zinc-oxide	Paclitaxel + cisplatin	---	Head and neck squamous carcinoma cells	Hackenberg *et al*. 2012
	Silver nanoparticles	---	---	Embryonic neural stem cells	Liu *et al*. 2015
Dendrimers	Polyamidoamines (PAMAM)-peptide HAIYPRH (T7)	---	pDNA	Bel-7402 Liver cancer cells	Somani *et al*. 2015
	PAMAM Dendrimer-FITC oligo complexes		siRNA	Cervical cancer cells	Dutta *et al*. 2010
Micelles	Folic acid	Paclitaxel	---	U14 Cervical cancer cells	Feng *et al*. 2012

1.8.1. Cellular barriers

At the cellular level there are various biological barriers that gene carriers need to overcome (Figure 10). These include cellular uptake and endosomal escape, intracellular trafficking, therapeutic molecule unpacking and biocompatibility. Complexes may be internalized via endocytosis after electrostatic binding to the anionic proteoglycans on the target cell membrane. The different endocytic pathways define the intracellular routes. Currently, clathrin-mediated endocytosis is the most characterized pathway, during which clathrin-coated pits pinch of the cell membrane and fuse with endosomes. Vesicle acidification continues when endosomes mature to lysosomes, with reduction of pH to around 5. Thus, the ability for the complexes to escape from enzymatic degradation in the endosomal low pH environment is paramount to successful gene delivery. (Teo *et al*. 2016)

For the polyplexes that escape out of the endosome into the cytosol, where is abundant nucleolytic enzymes, protection of nucleic acids is mandatory. For the specific case of pDNA, although the exact mechanism by which pDNA travels to the nucleus and is expressed is still under investigation, researchers have suggested that pDNA travels on the microtube network driven by microtubule-associated motor proteins to reach the nucleus. (Teo *et al*. 2016)

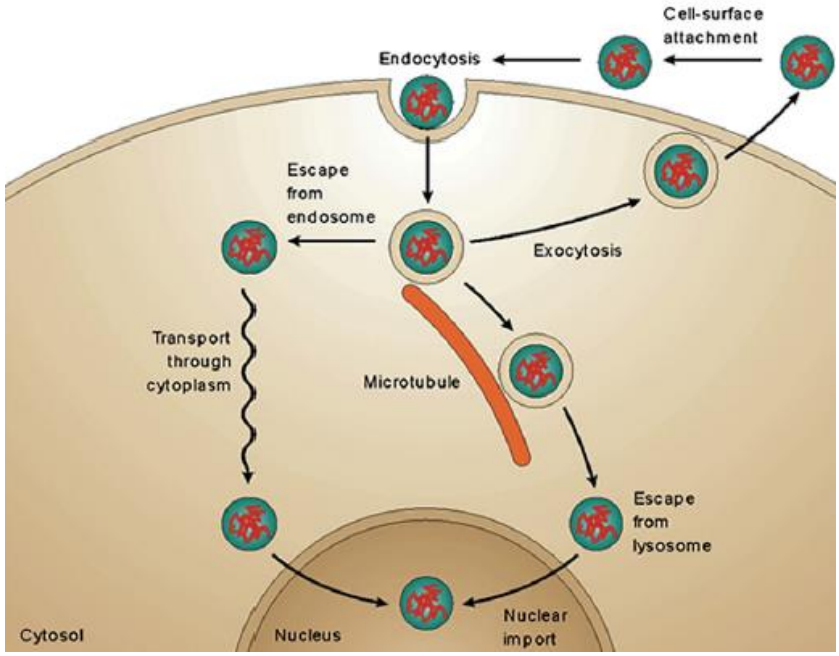

Figure 10: Barriers to intracellular trafficking of gene delivery systems. (Adapted from (Teo *et al*. 2016))

1.9. Cell penetrating peptides

Many peptides have been developed over recent years because they present the ability to penetrate the plasma membrane without compromising their integrity. These peptides are normally short (less than 30 amino acids), frequently rich in basic amino acids residues like

arginine residues, resulting in positively net charged. The cationic profile of cell penetrating peptides (CPP) is the key factor for their interaction with nucleic acids, giving rise to the formation of micro or nanometer complexes. CPPs are advantageous over other translocation methods because they possess high cellular permeability rates, ability to translocate into a wide spectrum of cell types, large cargo capacity and low cell toxicity associated with no immunological response. (Costa *et al*. 2019; Silva, Almeida, and Vale 2019)

The most publicized peptides have been the anionic membrane destabilizing peptide, GALA, which requires conjugation of a positively charged ligand to facilitate delivery of nucleic acid. On the other hand, CADY, KALA and RAWA are CPP which allow independent delivery of nucleic acids. (Bennett *et al*. 2015)

1.9.1 GALA and KALA peptides

Perhaps one of the most revolutionary peptides is GALA. It is fusogenic in nature and the seven EALA repeats confers α-helicity linked to pH responsiveness, realized through excellent endosomal disruption. Due to the spacing of the charged residues this peptide is capable of taking on the conformation of an amphipathic α-helix at a lower pH. However, due to its anionic nature, it cannot condense and protect nucleic acids. Coating of cationic complexes with GALA peptide, however, has proven successful at facilitating the endosomal escape of multi-functional delivery systems which are capable of binding and delivering nucleic acids intracellularly. (McCarthy *et al*. 2014)

To that end, KALA was the first artificially designed peptide of its kind with the glutamate residues of GALA replaced with lysine residues, enabling nucleic acid condensation and protection. The presence of multiple lysine residues in KALA means that in contrast to GALA, it has the ability to permeabilize membranes in a composition and pH dependent manner. The net charge of KALA increases with decreasing pH in the presence of neutral liposomes disrupting the α-helical structure and ablating any membrane permeabilizing activity. In the presence of negatively charged membranes however, the increased positive charge on KALA allows improved binding to the membrane and enhances its membrane permeabilizing activity. (McCarthy *et al*. 2014) However, circular dichroism (CD) studies showed that KALA undergoes a conformational change from an α-helical conformation to a mixture of α-helix and random coil as the pH is lowered. A decrease in the pH below 7 results in protonation of the histidine, charge neutralization of the glutamic acid side chains, and hence an increase in the net positive charge in the molecule which appears to disrupt the α-helix. *In vitro* studies also showed that KALA cause membrane destabilization and leakage in low-pH environments similar to that of the endosome. (Wyman *et al*. 1997)

1.9.2. RALA peptide

Arginine is found in naturally occurring DNA binding/condensing motifs with a higher frequency than lysine and has been shown to be a superior transfection agent. As arginine-rich peptide sequences exhibit improved internalization they have been widely exploited to aid the delivery of various gene delivery vehicles including peptide dendrimers, liposomes and polymer systems. McCarthy modified the RALA peptide, a 30-amino acid peptide where the KALA lysine residues were replaced with arginine, with decrease cytotoxicity, pH sensitivity and improved binding to outer leaflets of membranes and nucleic acids. (McCarthy *et al*. 2014)

RALA is an amphipathic peptide and exhibits an alpha helical structure (Figure 11) in a hydrophilic environment with hydrophobic amino acids on one face (leucine's) and hydrophilic on the other (arginine's), making it a suitable candidate for DNA condensation and efficient membrane perturbation. (Jain *et al*. 2015)

NH_2-WEARLARALARALARHLARALARALRACEA-COOH

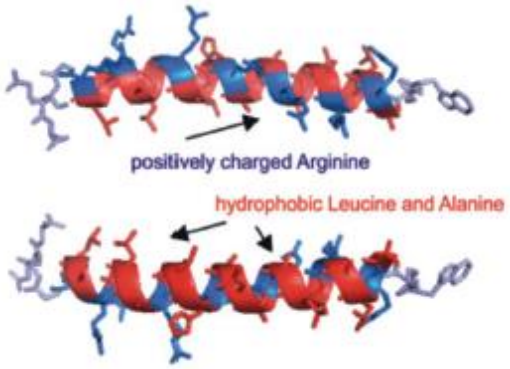

Figure 11: RALA primary and secondary structure. (Adapted from (Udhayakumar *et al*. 2017))

Arginine is positively charged in neutral, acidic and most basic environments, making RALA more responsive to the low pH found in the endosome, causing α-helicity selectively in the endosome and theoretically minimizing toxicity and leading to endosomal disruption and release of the cargo into the cytosol. (Massey *et al*. 2016; Bennett *et al*. 2015)

This peptide when exposed to anionic nucleic acids and due to electrostatic interactions self-assembles into nanoscale particles suitable for cell membrane penetration facilitating the intracellular delivery of DNA across the cell membrane and promoting nuclear localisation of the DNA for transcription. (McCrudden *et al*. 2017; McCaffrey *et al*. 2016)

Characterization studies indicated that RALA does not affect viability *in vitro* and successful reporter gene delivery following systemic administration *in vivo*.(Bennett *et al*. 2015)

RALA has been applied at delivered plasmids encoding reporter genes, mRNA, siRNA, DNA vaccines, mRNA vaccines and small molecules demonstrating broad utility (Table 2). (McCrudden *et al*. 2018)

Table 2: Examples of other studies using RALA peptide as carrier.

Nanocarrier	**Genetic agent**	**Cell line**	**References**
RALA-PLA-PEG	pDNA	ZR-75-1 Breast cancer cells	Jain *et al*. 2015
RALA	pEGFP-N1	ZR-75-1 Human breast cancer cells and PC-3 human prostate cancer cells	McCarthy *et al*. 2014
RALA-poly(vinylpyrrolidone) (PVP)	pCMV-Luc and pEGFP-N1	NCTC-929 Fibroblast cells	McCaffrey *et al*. 2016
RALA	iNOS	Breast cancer cells	McCrudden *et al*. 2016
RALA	pFKBPL and siFKBPL	ZR-75-1 Breast cancer cells	Bennett *et al*. 2016
RALA	pFKBPL	ZR-75-1 Breast cancer cells	Bennett *et al*. 2015
RALA	iNOS	MDA-MB-231 Breast cancer cells	McCrudden *et al*. 2017
RALA	E6/E7 DNA	NCTC-929 Fibroblast cells	Ali *et al*. 2017
RALA	pDNA	NCTC-929 Fibroblast cells	Cole *et al*. 2018
RALA	mRNA	Dendritic cells	Udhayakumar *et al*. 2017
RALA	Bisphosphonates	PC3 Prostate cancer and MDA-MB-231 breast cancer cells	Massey *et al*. 2016

Chapter II - Aim of the thesis

The objective of this thesis consisted in the design and development of a peptide/plasmid DNA delivery system, its biological activity evaluation *in vitro* and the investigation of its potential cancer therapeutic effect as alternative to conventional therapies applied in clinical setting nowadays. The main idea was to restore the p53 normal function in the cell and regulate their cycle leading to apoptosis.

In order to achieve this objective, it was crucial the formulation of a system composed by plasmid encoding p53 tumour suppressor gene encapsulated by RALA peptide at different N/P ratios and characterize it in terms of morphology, size, surface charge, encapsulation efficiency and pDNA protection and stability. Posteriorly, the capacity of the developed systems for cell uptake and internalization must be evaluated. Genetic expression, p53 protein expression and efficacy in inducing cancer cell apoptosis were also analysed in order to verify the therapeutic potential of this vector.

Chapter III - Materials and Methods

3.1. Materials

The pcDNA3-FLAG-p53, plasmid #10838, was purchased from Addgene (Cambridge, MA, USA). For the bacterial cultures, tryptone and yeast extract were obtained from Bioakar Diagnostics and *Luria-Bertani* (LB) medium in PanReac. For alkaline lysis and pDNA purification a protocol optimized by our research group and described in the literature was used. (Diogo *et al*. 2000; Sambrook, Fritsch, and Maniatis 1989) In electrophoresis assays, GreenSafe reagent (GreenSafe Premium) was obtained from NZYTech Lda. For systems formulation, RALA peptide (N-WEARLARALARALARHLARALARALRACEA-C) with average M_w = 3328.30 MM and a purity of 95.02 % was obtained from Biomatik. 3-(4,5-dimethylthiazol-2-yl)-2,5-diphenyltetrazolium bromide (MTT) and fluorescein isothiocyanate (FITC) were obtained from Sigma-Aldrich (St Louis, M.O., EUA). 4′,6-diamidino-2-phenylindole (DAPI) was purchased from Invitrogen (Carlsbad, CA). Normal human dermal fibroblasts (NHDF), Ref. C-12302 (cryopreserved cells), and cancer HeLa cells were purchased from PromoCell and Invitrogen, respectively. For PCR methodology, Taq polymerase and $MgCl_2$ were obtained from NZYTech, Lda. For western blot assay anti-p53 antibody (Santacruz Biotechnology, DO-1: sc-126), anti-mouse IgG–peroxidase antibody (Sigma-Aldrich, A3682), BAX antibody (Cell Signalling, #2772), anti-rabbit IgG–peroxidase antibody (Sigma-Aldrich, A0545), monoclonal anti-ß-actin−peroxidase antibody (Sigma-Aldrich, A3854), Pierce™ ECL Western Blotting substrate (Thermo Scientific) and NZYcolour Protein Marker II (NZYTech, Lda. - Genes and Enzymes, Lisbon, Portugal) were acquired. All solutions were freshly prepared by using ultra-pure grade water, purified with a Milli-Q system from Millipore (Billerica, MA, USA).

3.1.1. Plasmid DNA

The 6.59 kbp plasmid pcDNA3-FLAG-p53 used in this set of assays encodes for the human p53 protein, for the ampicillin resistance gene and the neomycin selectable marker (Figure 12).

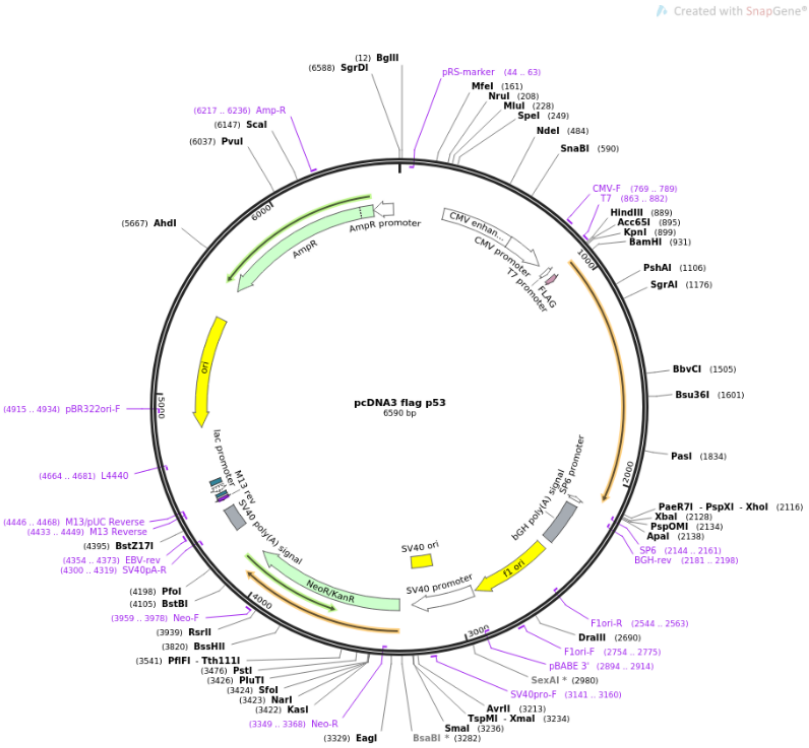

Figure 12: Plasmid pcDNA3-FLAG-p53. (Adapted from Addgene)

3.2. Methods

3.2.1. Bacterial growth conditions and plasmid production

The plasmid was amplified intracellularly in *Escherichia coli* (*E. coli*) DH5*α*. Initially, the strain was inoculated in LB-agar plates containing ampicillin (30 µg/mL) and it was left to grow overnight at 37 ºC. After the growth in solid medium, some colonies were transferred to an Erlenmeyer with capacity of 250 mL, containing 62.5 mL of *Terrific Broth* (TB) liquid pre-fermentation medium, composed by 20 g/L tryptone, 24 g/L yeast extract, 4 mL/L glycerol, 0.017 M KH_2PO_4 and 0.072 M K_2HPO_4 and supplemented with 30 µg/mL ampicillin. The cells were left to grow in an orbital agitator (Agitorb 200 da Aralab, Albarraque, Portugal) at 250 rpm and 37 ºC. When an optic density (OD) of approximately 2.6 was reached, a certain volume of pre-fermentation medium was transferred to 125 mL of TB fermentation medium included in two erlenmeyers of 500 mL. After 16/18 h (OD ~ 9, at the late log phase), bacterial growth was suspended, and the total volume of fermentation divided for 50 mL Falcon tubes for posterior cell collection by centrifugation at 1000 g for 4 min and pellets storage at -20 ºC until use.

3.2.2. Plasmid extraction and purification

Posteriorly to production, plasmid was extracted/recovered by the modified alkaline lysis method and purified according to the optimized protocol by our research group. (Diogo *et al.* 2000; Sambrook, Fritsch, and Maniatis 1989) The modifications were made to NZYTech Plasmid Maxi kit manufacturer protocol in order to optimize the plasmid recovery rate. Initially, the

bacterial pellet was resuspended in 10 mL of P1 buffer (50 mM of Tris-HCl at pH = 8.0, 10 mM of EDTA hydrated and 100 µg/mL RNase A) and then in 10 mL of P2 buffer (200 mM of NaOH and 1 % of SDS (w/v)). To promote cell lysis the tubes were carefully inverted and incubated at room temperature for 5 min. The lysis step was stopped with the addition of 10 mL of P3 buffer (3.0 M potassium acetate at pH = 5.0 and 1 % of SDS (w/v)) and incubation on ice for 20 min. Then, tubes were centrifugated for 30 min (20 000 g and 4 ºC), supernatant was transferred to new tubes and centrifugated 20 min (20 000 g and 4 ºC). Thus, some precipitated contaminants are eliminated, such as cell debris, gDNA and proteins. Afterwards, the columns (anion-exchange resin with L-methionine-agaroses matrix) were regenerated with a regeneration solution (0.15 % Triton X-100 and 3 M NaCl) and equilibrated with QBT buffer (0.75 M NaCl, 50 mM MOPS, 15 % isopropanol (v/v), 0.15 % Triton X-100 (v/v) at pH = 7.0). The supernatants were added to columns and the proteins and low molecular weight molecules were removed by the addition of a buffer with low salt content (0.5 M NaCl). Elution of plasmid DNA was promoted directly to empty centrifuge tubes by the addition of a buffer with higher salt concentration (1.25 M NaCl). The pDNA was precipitated by the addition of 0.7 volumes of isopropanol, followed by incubation on ice for 20 min. The obtained samples were subjected to centrifugation (16 000 g, 4 ºC and 10 min) and the pellet was resuspended in 1 mL of Tris base (10 mM, pH 8.0) and stored at -80 ºC. The 260/280 nm absorbance ratio was found to be above 1.8. The samples were also analysed by electrophoresis for 30 min under 120 V in 1 % agarose gel containing ethidium bromide with Tris-acetate-EDTA (TAE) (40 mM Tris base, 20 mM acetic acid and 1 mM EDTA, pH 8.0) running buffer and GreenSafe as colorant to verify the main conformation of the plasmid and possible contaminations.

3.2.3. Preparation of RALA/pDNA complexes

RALA was synthetized by solid-state synthesis (fluorenylmethyloxycarbonyl, FMOC) and supplied as a desalted lyophilized powder. Reconstitution was in ultrapure grade water to a stock concentration of 0.5 mg/mL. Aliquots were stored at -20 °C until use.

The systems were prepared at various nitrogen/phosphate (N/P) ratios, ranging from 1 to 50, considering the mass per charge ratio of DNA (330 g/mol, relative to one phosphate group) and RALA (44 g/mol, correspondent to one amine group). Nanoparticles were formed by adding an appropriate and calculated volume of peptide solution, dropwise at vortex for 60 s, to a fixed amount of pDNA (1 µg) (at ratio N/P 1 were added 2.9 µg of RALA peptide to 1 µg of pDNA) and left for 30 min at room temperature to allow complexes formation.

3.2.4. Determination of encapsulation efficiency (EE)

After complexes formation they were centrifuged at 10 000 rpm for 20 min at 4 ºC and the pellet contained the pDNA based vectors was recovered. The amount of non-bound pDNA in

supernatant was determined spectrophotometrically measuring the absorbance of the supernatant at 260 nm using a NanoPhotometer™ (Implen GmbH, Munich, Germany). The pDNA encapsulation efficiency (EE) for each system was calculated by the following equation:

$$EE\ (\%) = [(\text{Total Amount of pDNA} - \text{non-bound pDNA})/\text{Total amount of pDNA}] \times 100 \quad (1)$$

3.2.5. Scanning Electron Microscopy (SEM)

The geometry and morphology of pDNA/RALA particles was investigated by Scanning Electron Microscopy (SEM). Freshly prepared pDNA vehicles were centrifuged (10 000 rpm, 20 min, 4 °C), the pellet recovered and then suspended in an aqueous solution containing 40 µL of 2 % tungsten. The samples were diluted 1:20 in ultra-pure grade water, 10 µL pipetted to roundly shaped coverslip (10 mm) and left dry overnight at room temperature. In the following day, the samples were mounted on aluminium supports, fixed with double-sided adhesive tape and sputter coated with gold using an Emitech K550 (London, England) sputter coater. A scanning electron microscope, Hitachi S-2700 (Tokyo, Japan) with accelerating voltage of 20 kV at various magnifications was used to determine the morphology of nanoparticles.

3.2.6. Particle size and zeta potential measurements

The pellet containing polyplexes was suspended in 1 mL of ultra-pure grade water as a dispersant medium. The average particle size and the zeta potential of pDNA based vectors were determined by Dynamic Light Scattering (DLS), at 25 ºC, using a Zetasizer Nano ZS (Malvern Instruments, UK). For data analysis, dispersant viscosity and refractive index are considered the same as those for pure water at 25 ºC: 0.8905 mPa s^{-1} and 1.333, respectively. Dynamic light scattering (DLS) using a He-Ne laser 633 nm with non-invasive backscatter optics (NIBS) and electrophoretic light scattering using M3-PALS laser technique (Phase Analysis Light Scattering) were applied for systems size and charge investigation, respectively. Zeta potential was determined in 5 % glucose with 1 mM NaCl. The Malvern Zetasizer software v 6.34 was used to obtain and treat the data.

3.2.7. Fourier-Transformed Infrared Spectroscopy (FTIR) analysis

To confirm the formation of pDNA complexes a Fourier-transform Infrared Spectroscopy (FTIR) assay was performed. The pellet of polyplexes from various assays was suspended in 10 µL of ultra-pure grade water and joined together to further analysis. The spectra were acquired by using a Nicolet iS10 FTIR spectrophotometer (Thermo Scientific, Waltham, MA, USA) operated in ATR (Smart iTR diamond ATR) mode with an average of 120 scans, a spectral width ranging from 4000 and 525 cm^{-1} and a spectral resolution of 32 cm^{-1}. For comparative purposes, the spectra of pDNA and RALA were also acquired.

3.2.8. Circular Dichroism (CD)

To verify peptide and systems secondary structure circular dichroism (CD) spectra were acquired on a JASCO L-815 spectropolarimeter (Jasco International Co. Ltd., Japan) in quartz cells with an optical path of 1 mm for RALA in solution (40 μM) or in the presence of RALA/pDNA formulations at different N/P ratios (2, 5 and 10). Spectra were obtained from 3 accumulations in the wavelength range between 190 and 260 nm with a data pitch of 0.5 nm, a speed of 50 nm/min, a bandwidth of 1 nm and a standard sensitivity.

3.2.9. Plasmid DNA protection studies

RALA/pDNA complexes were prepared and the pellet resuspended in 25 uL of Dulbecco´s Modified Eagle´s Medium (DMEM) medium containing 10 % fetal bovine serum (FBS) at 37 °C for 1, 4, 6 and 12 h.

Then, polyplexes were resuspended in 12.5 μL phosphate buffered solution (PBS) buffer, pH 7.4, and 1.5 μL of 10 % FBS and incubated at 37 °C for 30 min, 2 and 4 h.

Furthermore, pDNA/RALA nanoparticles were incubated with 20 μL of trypsin and incubated at 37 °C for 1 and 3 h.

Finally, nanoparticles were incubated with 10 μL of DNase I solution (4.5 mg/mL) at 37 °C for 1 h. After this period, 4 μL of 0.25 M EDTA was added to inactive the enzyme and stop the reaction and samples were incubated for 15 min. Subsequently, the condensed DNA was decomplexed from RALA by addition of 1.5 μL of 10 % SDS and incubated for more 10 min.

Samples of all studies were electrophoresed for 30 min under 120 V in 1% agarose gel. Naked p53-encondig pDNA was used as control.

3.2.10. Cell culture

Cancer HeLa cells from cervical adenoma were grown in 25 cm^3 T-flasks with Dulbecco´s Modified Eagle´s Medium with High Glucose (DMEM-HG) (Sigma) supplemented with 10 % heat inactivated FBS, 0.5 g/L sodium bicarbonate, 1.10 g/L HEPES and 100 μg/mL of streptomycin and 100 units/mL of penicillin (Sigma) at 37 ºC in a 95 % O_2/5 % CO_2 humidified atmosphere, until confluence was attained. Afterward cells were sub-cultivated each 7 days to maintain their exponential growth.

3.2.11. Cytotoxicity analysis

The biocompatibility of the systems was evaluated on fibroblast cells by means of MTT (3-[4,5-dimethyl-thiazol-2-yl]-2,5-diphenyltetrazolium bromide) assay. This colorimetric method quantifies the metabolic active cells. Before cell seeding, the 96-well plates were ultraviolet

(UV) irradiated for 30 min. Human fibroblast cells were plated at confluency at a density of 1×10^4 cells per well and grown at 37 °C in a 95 % O_2/ 5 % CO_2 humidified atmosphere. The polyplexes were applied to the well plates. After 24 and 48 h of incubation, the redox activity was assessed through the reduction of the MTT. 100 µL of MTT dye solution (0.05 mg/mL in Krebs) was added to each well, followed by incubation for 2 h at 37 °C, in a 5 % CO_2 atmosphere. The medium was aspirated, and the cells were treated with 50 µL of isopropanol/HCl (0.04 N) for 30 min. Absorbance at 570 nm was measured using a Biorad Microplate Reader Benchmark. The spectrophotometer was calibrated to zero absorbance using the culture medium without cells. The relative cell viability (%) related to control wells was calculated by $[A]_{test}$ / $[A]_{control}$ × 100, where [A] test is the absorbance of the test sample and [A] control is the absorbance of control sample. All the experiments were repeated three times in triplicate. The statistical analysis of experimental data used the Student's t-test and the results were presented as mean ± standard deviation. Statistical significance was accepted at a level of $p < 0.05$.

MTT assay was also applied to measure the cellular viability of cancer cells after its incubation with the developed RALA/pDNA vectors at different N/P ratios 2, 5 and 10, but using a density of 2×10^5 cells per well.

3.2.12. *In vitro* transfection studies

3.2.12.1. Plasmid labelling with FITC

Plasmid was labelled with fluorescein isothiocyanate (FITC) fluorochrome. To 20 µL (2 µg) of plasmid solution was added 63 µL of labelling buffer and 2 µL of FITC (total volume of 85 µL). The samples were placed under constant stirring for 4 h at 4 ºC and protected from light. One volume of 3 M sodium chloride (85 µL) and 2.5 volumes of 100 % ethanol (212.5 µL) were added, and samples with the stained plasmid incubated overnight or for 30 min at -20 ºC. Then, the solution was centrifugated at 12 000 g for 30 min and the supernatant removed. The pellet was further washed with 75 % ethanol and centrifugated for more 10 min. This step was repeated until the loss of orange colour from solution. After removing the ethanol, the pellet was suspended in 20 µL of ultra-pure grade water for posterior formulation.

3.2.12.2. Fluorescence confocal microscopy

For the fluorescence confocal microscopy assays, HeLa cells were seeded at a density of 1×10^5 cells/well onto the poli-L-lysine coverslip 12-well plate and grown in 1.5 mL of complete medium at 37 °C in a 5 % CO_2 humidified atmosphere. After 24 h and 12 h, at least, before transfection the complete medium was replaced by medium without FBS and without antibiotic (simple DMEM-HG medium), in order to promote transfection. HeLa cells were transfected with the several polyplexes (1 µg pDNA FITC labelled were added to each well) and incubated for a period of 2, 4 and 6 h. To fix the cells, they were incubated with 1 mL of 4 % paraformaldehyde

(PFA) for a period of 10 min. To stain the nucleus, cells were incubated with 120 µL of DAPI for 10 min. Cells were then mounted by placing the round shaped lamellas in a lamina with the help of Entellan solution and visualized through confocal microscopy (Carl ZEISS LSM 710, Oberkochen, Germany). Between any incubation period, cells were always washed three times with PBS solution. All procedures were performed at room temperature and in the dark to ensure probes efficacy. All images were obtained using at the same time DAPI and FITC correspondent lasers and image edition was performed with Zen 2.6 (blue edition) software.

3.2.12.3. Live cell imaging

For the live cell imaging assay, plasmid DNA was labelled and complexed as described before. HeLa cells were seeded at a density of 25 000 cells/well onto the µ-slide 8 well (Ibidi, Martinsried, Germany) and grown in 275 µL of complete medium at 37 °C in a 5 % CO_2 humidified atmosphere. After 24 h and 12 h, at least, before transfection the complete medium was replaced by simple medium. Cells were washed once with PBS and nucleus stained with 50 µL of DAPI for 10 min. Then the cells were transfected with the several polyplexes (0.25 µg pDNA FITC labelled were added to each well) and incubated for a period of 2, 4 and 6 h. Through LSM 710 confocal laser scanning microscope (Carl ZEISS, Oberkochen, Germany) and with a 40x ampliation was possible to observe cellular and nuclear internalization of pDNA at the three different end points. Z-stacks option was used to confirm internalization after 4 h of transfection. All the images were acquired using at the same time DAPI and FITC correspondent lasers and cells were maintained at 37 ºC with 5 % CO_2.

3.2.13. Gene transcription

3.2.13.1. RNA extraction

Qualitative mRNA expression of p53 was analysed using reverse transcription polymerase chain reaction (RT-PCR). For PCR assays, after 4 h of transfection, the cell culture medium was replaced with complete medium to stop the transfection and the cells were allowed to incubate for 24 h. To extract RNA, the medium was removed, and cells were washed 3 times with PBS. Untreated cells were used as control. To extract total RNA, the cells were lysed through the addition of 250 µL of TRIzol (Thermo Scientific, Lisbon, Portugal) and incubated for 5 min to room temperature. 50 µL of chloroform were added and samples vigorously agitated to separate the different biomolecules present in the sample. After 10 min of incubation, at room temperature, were centrifugated at 4 °C for 15 min at 12 000 g. The aqueous phase was carefully removed, and the RNA precipitated with 125 µL of iced isopropanol. The samples were kept on ice for more 10 min and centrifugated at 4 °C for 15 min at 12 000 g. The pellet was suspended in 125 µL 75 % ethanol (prepared in diethylpyrocarbonate (DEPC) water) to remove the organic compounds and centrifuged at 4 °C for 5 min at 12 000 g. The supernatant was discarded, and the pellet allowed to dry to be rehydrated with 20 µL of DEPC water. The RNA

samples were quantified by using a Nanophotometer™ and additionally they were run on an agarose gel (1%) and analysed by electrophoresis to detect possible contaminations with gDNA or RNA degradation.

3.2.13.2. cDNA synthesis

The cDNA synthesis was performed using Xpert cDNA Synthesis kit (GRiSP Research Solutions, Porto). In a RNase free tube was added 1 µL of dNTP's, 1 µL of Random primer, 1 µg of RNA Template and RNase free water until a total volume of 14.5 µL. The samples were incubated at 65 °C for 5 min and posteriorly placed on ice for 2 min. Thereafter, 4 µL of buffer, 0.5 µL of RNase Inhibitor and 1 µL of Xpert RTase were added and the mixture homogenised softly. Using a thermocycle the samples were incubated at 25 °C during 10 min, 50 °C 50 min and 85 °C 5 min. The cDNA samples were used as PCR template or stored at -20 ºC.

3.2.13.3. Reverse transcription polymerase chain reaction (RT-PCR)

PCR amplification of p53 cDNA were carried out adding in each PCR reaction 1 µL of synthesized cDNA, 3.95 µL of RNase free water, 0.40 µL of primer reverse (5-CCT CAT TCA GCT CTC GGA AC-3) and primer forward (5-CCT CAC CAT CAT CAC ACT GG-3) to detect p53 transcripts, 0.5 µL of $MgCl_2$ and 6.25 µL of polymerase DNA Taq. The samples were homogenized, and a mini spin was performed. Samples were then placed in a T100™ Thermal Cycler (Bio-Rad Laboratories, Inc, Hercules, California, USA), with the following conditions: denaturation (95 °C for 40 s), annealing (60 °C for 30 s), and extension (72 °C for 1 min) for 29 cycles. Assays were performed in triplicate. PCR products were analyzed by electrophoresis and visualized in UVItec Gel documentation system under UV light (UVItec Limited, Cambridge, United Kingdom).

3.2.14. Western Blot

The qualitative levels of p53 protein expression in non-transfected and transfected cells with the various vectors were determined by western blot analysis. For this assay, after 4 h of transfection, the cell culture medium was replaced with complete medium and the cells were allowed to incubate for 48 h.

3.2.14.1. Protein extraction

To extract the total protein from cells, cells were washed 3 times with cold PBS, scrapped with a cell scrapper and reserved in microtubes. Then, the microtubes were centrifuged at 10 000 g for 3 min at 4 ºC. The supernatant was discarded and 30 µL of complete lysis medium (25 mM Tris, 2.5 mM EDTA, 1 % Triton X-100, 2.5 mM EGTA, 1 mM phenylmethylsulfonyl fluoride (PMSF), 10 µL/mL complete EDTA free protease inhibitor cocktail (Roche, USA)) was added and homogenate incubated 10 min on ice. Then tubes were centrifugated at 10 000 g for 1 min and supernatant removed for a new tube.

3.2.14.2. Protein quantification

Protein concentration was measured using Pierce 660 nm Protein Assay Reagent (Thermo Scientific USA). In summary, 2 µL of sample, 8 µL of ultrapure grade water and 150 µL of Pierce reagent were prepared in a microplate for each sample, in triplicate. Microplate was manually agitated for 1 min and then incubated for 5 min at room temperature. Absorbance was then recorded at 660 nm. Afterwards, a calibration curve was constructed, by using bovine serum albumin (BSA) (Thermo Scientific, USA) as a standard protein (25-2000 µg/mL) (Figure 14).

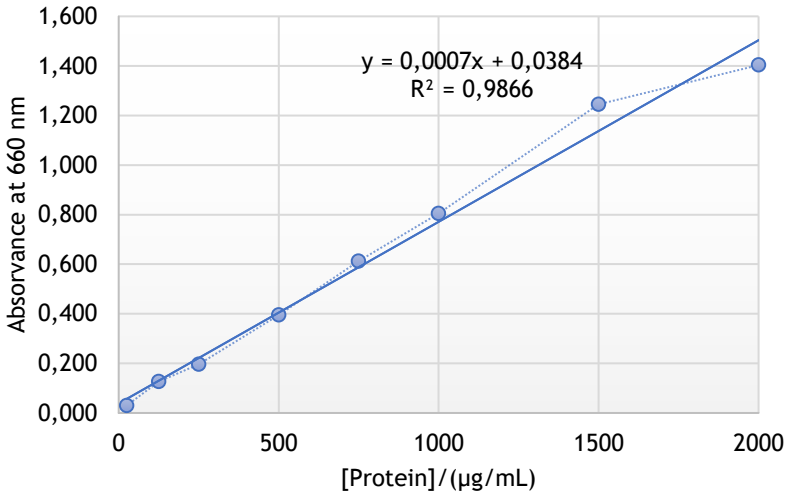

Figure 13: Calibration curve obtained with protein standards (25-2000 µg/mL).

3.2.14.3. Polyacrylamide gel electrophoresis

Sodium dodecyl sulphate-polyacrylamide gel (SDS-PAGE) electrophoresis was performed using 10 % polyacrylamide resolving gel and 5 % polyacrylamide stacking gel. The samples were prepared with 50 µg of each protein sample, whose volume was calculated through the calibration curve constructed by protein quantification, and 5 µL of loading buffer, followed by 10 min of denaturing at 95 ºC. Afterwards the electrophoresis was carried out first at 95 V, for 15 min, and then at 130 V, for more 100 min.

3.2.14.4. Electroblotting

Protein gel electrotransfer is based on the transference of total proteins of an electrophoresis gel to a polyvinylidenedifluoride membrane (PVDF). Electroblotting was carried out with the protein gel resulting from previous electrophoresis. Membrane activation was performed with methanol. Electrotransfer was performed at 0.75 A and 100 V for 105 min. Afterwards, the membrane was washed 3 times with washing buffer (10 mM Tris, 68.45 mM NaCl, 0.1 % Tween 20) for 5 min and blocked by incubation with 5 % BSA at room temperature for 1 h. Afterwards, the membrane was washed 3 times for 5 min and incubated overnight at 4 ºC with anti-p53

primary antibody (1:200 in washing buffer and 5 % BSA) (Santa Cruz Biotechnology) and BAX antibody (1:1000 in washing buffer and 5 % BSA) (Cell Signalling). Hereafter, the membrane was washed 3 times for 5 min and incubated at room temperature with anti-mouse IgG–peroxidase antibody (1:5000 in washing buffer and 5 % BSA) (Sigma Aldrich) and anti-rabbit IgG–peroxidase antibody (1:5000 in washing buffer and 5 % BSA) (Sigma Aldrich), respectively, for 1 h. Then, the membrane was washed more three times for 5 min and incubated for 5 min with ECL substrate (Thermo Scientific Inc., USA) to be visualized in ChemiDoc™ XRS system (BioRad, UK) and analysed with the Image Lab software (BioRad). To have a housekeeping (control), the membrane was incubated in monoclonal anti-ß-actin−peroxidase antibody (1:20 000 in washing buffer) (Sigma-Aldrich) for more 90 min, washed 3 times and incubated for 5 min with ECL substrate.

3.2.15. Protein quantification

After transfection mediated by the developed RALA systems, cytosol has been isolated from the other cellular fractions through the use of the Mitochondria Isolation Kit for Cultured Cells (#89874, Thermo Fisher Scientific Inc., Rockford, USA), following the manufacturer´s instructions in order to separate essentially the mitochondria and the cytosol. The levels of p53 in the cytosol of HeLa cells were quantified by using the p53 pan ELISA kit (Roche Applied Science), following all the instructions provided by the manufacturer. The p53 concentration can be determined by measuring the absorbance at 450 nm using Shimadzu UV-Vis 1700 spectrophotometer. All the experiments were repeated three times in triplicate. Student's t-test was used to determine significance, and the results were presented as mean ± standard deviation (SD).* $p < 0.05$, ** $p < 0.01$.

3.2.16. Caspase-3 activity

The activity of caspase-3 was measured using the ApoAlert™ Caspase-3 Colorimetric assay kit (Clontech Lab. Inc, A. Takara, USA), following the provided instructions. Briefly, HeLa cells were serum starved and incubated with RALA/pDNA systems for 24 h. Incubation with 1 μM of staurosporine during the same time period has been considered as positive control. The activity of caspase-3 was assayed by colorimetric detection, at 405 nm, of p-nitroaniline (pNA) after cleavage from the peptide substracte DEVD-pNA.

3.2.17. TUNEL assay

Apoptotic cells were detected using the in-situ cell death detection kit (Roche Diagnostics, Basel, Switzerland), based on the terminal deoxynucleotidyl transferase-mediated dUTP nick end labelling (TUNEL) method and in accordance with the manufacturer's instructions. 1×10^5 HeLa cells were plated in a 12 well plate, transfected with nanoparticles for 4 h and then maintained in complete medium more 48 h. Then, cells were washed 2 times with PBS, left to

dry during 5 min at room temperature and fixed with 1 mL of 4 % PFA, washed more 2 times, permeabilised with 1 mL of a solution consisting of 0.1 % Triton X-100 in 0.1 % sodium citrate, washed more 2 times and labelled with 75 uL of TUNEL reaction mixture for 1 h. Coverslips were then washed more 2 times and incubated for 10 min with 120 µL of DAPI, washed once more, mounted onto microscope slides and visualised by confocal microscopy. Coverslips with label solution (not containing the terminal transferase) were used as negative controls, and a coverslip incubated 10 min at room temperature with recombinant DNase I before labelling procedures and incubation with staurosporine (Sigma-Aldrich) 1 µM were used as positive controls, as recommended by the manufacturer.

Chapter IV - Results and discussion

4.1. The properties of RALA/p53 complexes

RALA is a 30mer cationic arginine-rich peptide. Due to its positively and high charge density it binds strongly, mainly by electrostatic interactions, to negatively charged phosphate backbone of nucleic acids and condense/compacts them spontaneously into nano-sized complexes. (Jain *et al*. 2015; Costa *et al*. 2015) This ability of RALA to strongly bind, interact and consequently condense the DNA has been widely recognized and explored to be employed in the formulation of transporting agents for nucleic acids delivery. Following this strategy, in the present study we started by forming pDNA based particles by direct addition of RALA peptide solutions to the aqueous pDNA solution. This is a simple and fast way to produce nanoparticles with easy control of particle size and composition, along with several possibilities to modify the particle surface state and overall homogeneity. (Santos *et al*. 2014)

Similar to other systems reported in the literature, the N/P ratio considered at complex formulation step was found to deeply influence the pDNA condensation profile. (Costa *et al*. 2015; Costa *et al*. 2019; Konate *et al*. 2019) This behaviour was investigated by agarose gel electrophoresis. The results, for a broad range of N/P ratios, are presented in figure 14.

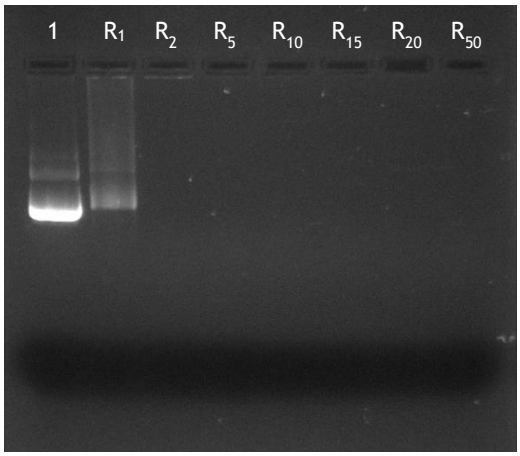

Figure 14: RALA/pDNA complexation behaviour at various N/P ratios investigated by agarose gel electrophoresis. The samples were loaded at the application site at the upper end of the image and the lower end is the cathodic end. Lane 1: pDNA control; lane 2: RALA/pDNA N/P 1; lane 3: RALA/pDNA N/P 2; lane 4: RALA/pDNA N/P 5; lane 5: RALA/pDNA N/P 10; lane 6: RALA/pDNA N/P 15; lane 7: RALA/pDNA N/P 20; lane 8: RALA/pDNA N/P 50.

The interaction of RALA with pDNA based plasmid leads to the immobilization of pDNA in a molar ratio-dependent manner. For nanoparticles prepared at N/P ratio of 1, RALA is unable to

efficiently condense the plasmid as seen by the migration down the gel by non-encapsulated pDNA. From N/P ratio 2 upwards, RALA efficiently neutralizes the p53-encoding pDNA negative charge and pDNA cannot migrate through the agarose gel remaining in the wells. An increment on N/P ratio parameter and, therefore, on amine positive charges of arginine residues, strengths the interaction between the peptide and pDNA, greatly condensing the latter. This result on pDNA immobilization follows the same trend already documented for similar RALA/pDNA based vectors. (McCrudden *et al*. 2018; McCarthy *et al*. 2014; Jain *et al*. 2015)

Furthermore, FTIR spectra were recorded in order to identify and confirm the existence of inter and intra-molecular interactions between system components and to confirm the encapsulation of p53-enconding pDNA into the complexes. In figure 15 are represented the spectra for the plasmid, RALA peptide and RALA/pDNA nanoparticles formulated at N/P ratio of 10, and relevant information concerning their fine structure upon association can be described.

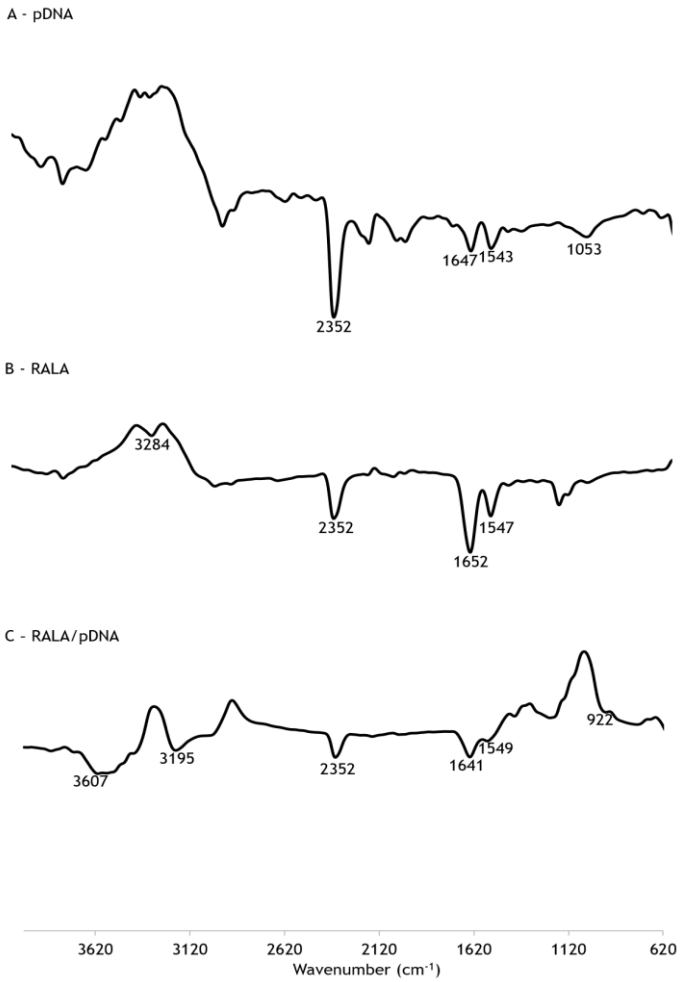

Figure 15: FTIR spectra (Transmittance (%) versus Wavenumber (cm^{-1})) of pDNA (A), RALA (B), and RALA/pDNA nanoparticles formulated at N/P ratio of 10 (C).

The spectrum of pDNA (15A) presents peaks in the region from, approximately, 1700-1500 cm^{-1} corresponding to the nitrogenated bases of plasmid, while the narrow band at 1053 cm^{-1} can be attributed to the carbonyl stretching vibration of furanose ring. (Mohsen 2011; Dev and Walters 1990) Figure 15B shows the RALA characteristic peaks, namely, the band at 3284 cm^{-1} from the C–H stretching and the bands at 1652 cm^{-1} and 1547 cm^{-1} from –COOH and amine groups, respectively. (Chalanqui *et al.* 2019; Dev and Walters 1990; Ikuta *et al.* 2014) The spectrum of RALA/pDNA complexes at N/P ratio of 10 is represented in Figure 15C. The nitrogen base region of pDNA overlaps with the characteristic amine bands of the peptide, and other regions must be analyzed to infer the interaction between pDNA and RALA. However, in this amine region some band shifts can be observed and, most probably, are a consequence of the complexation process. Moreover, the characteristic peak of RALA at 3284 cm^{-1} is shifted to lower wavenumber (3195 cm^{-1}) after nanoparticles formation. The absorbance peak at 922 cm^{-1} is indicative of the existence of DNA and the absence of the peak from vibration of furanose ring is also indicative of interaction involving the sugar-phosphate backbone of pDNA molecule. The band at 2352 cm^{-1} present in all spectra results from incomplete CO_2 purging of the spectrometer, as identified and reported by other authors, and are not related to the systems. (Petit and Puskar 2018)

To investigate the secondary structural conformation of RALA/pDNA complexes, circular dichroism (CD) spectra were recorded for both peptide and RALA/pDNA nanoparticles (Figure 16).

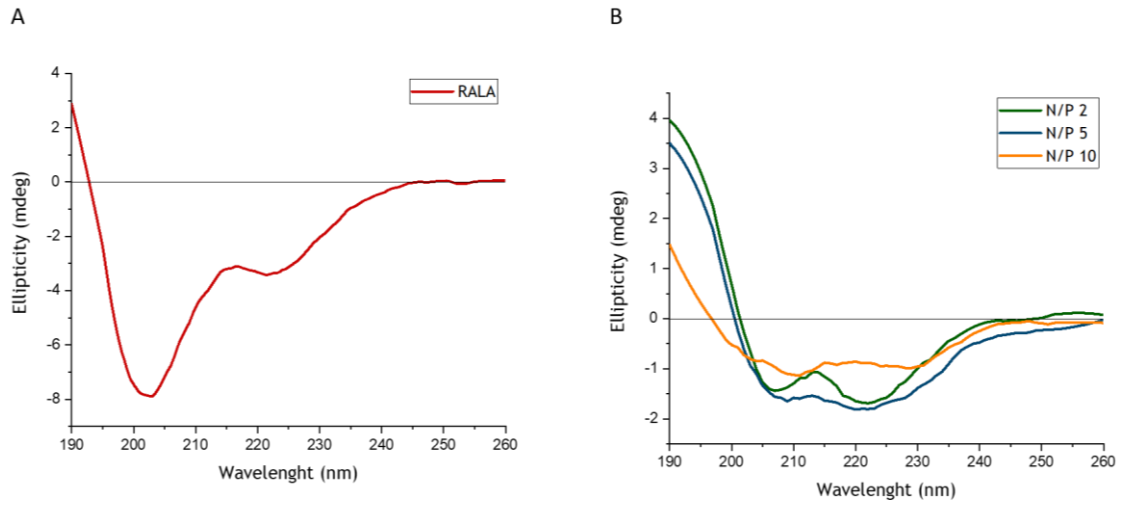

Figure 16: Representation of circular dichroism spectra of RALA peptide (40 μM) (A) and RALA/pDNA vectors at N/P ratio of 2, 5 and 10 (B). Helical conformation is characterized by the presence of one maximum at approximately 191 nm and two minima at 207 and 222 nm.

Spectrum of RALA peptide free in solution (Figure 16A) was mainly characterized by two minima at 203 nm and 222 nm, and a maximum at 190 nm indicative of a pronounced α-helical structure (maximum peak at around 191 nm and minima at 207 e 222 nm). CD spectra from the complexes

(Figure 16B) demonstrate that the α-helical structure characteristic of RALA peptide is maintained when complexed with the plasmid. However, the N/P ratio seems to influence the helicity of the complexes; while carriers at N/P ratio of 2 and 5 showed clear helical profiles, the spectrum from formulations at N/P ratio of 10 is less defined (Figure 16B). This observation may be linked with a different extent of interaction between RALA and pDNA at this ratio. The peptide conformational changes in RALA/pDNA complexes depending on N/P ratio is a quite interesting topic of research. This subject is already under investigation by our research team and, fortunately, will be reported in a near future.

The morphology of RALA/pDNA nanoparticles was analysed by scanning electron microscopy. Figure 17 shows images of these carriers prepared at N/P ratios of 1, 2, 5, 10, 15, 20 and 50.

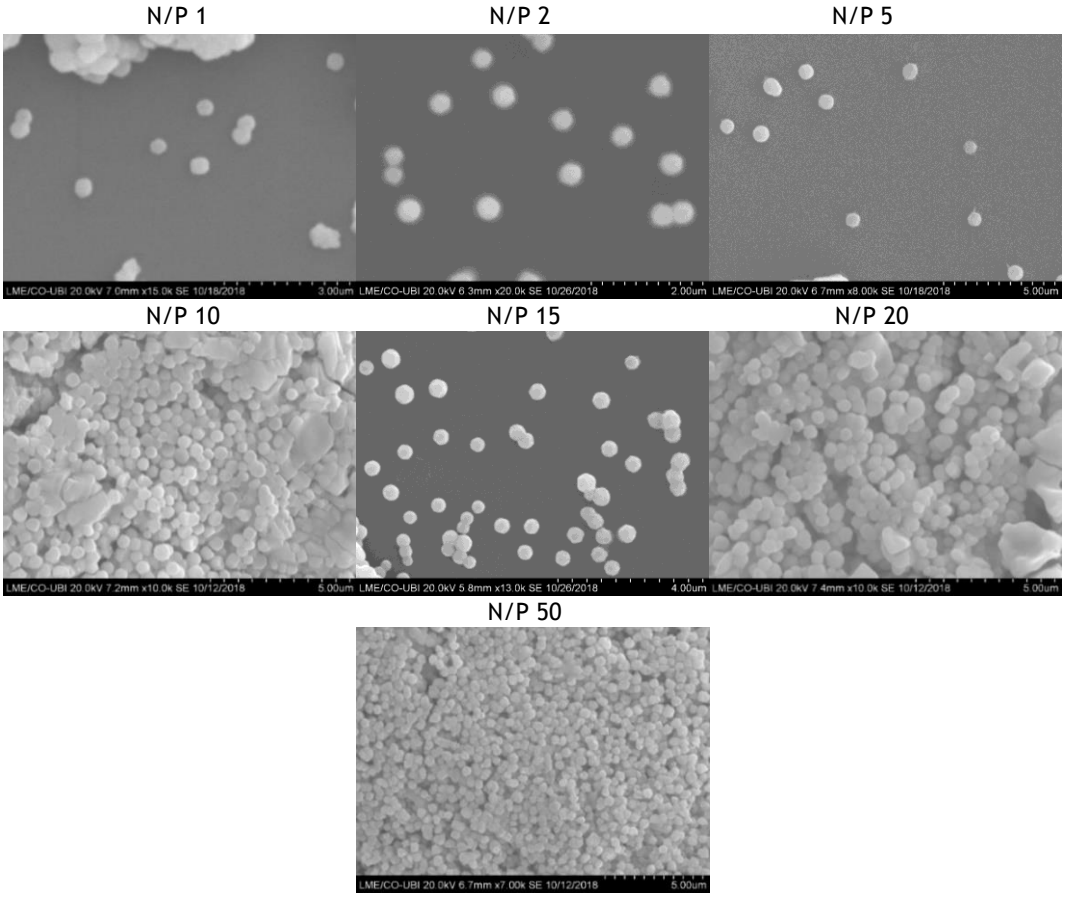

Figure 17: Scanning electron micrographs of RALA/p53 nanoparticles formulated at N/P ratios of 1, 2, 5, 10, 15, 20 and 50.

All the particles exhibit a spherical or oval shape displaying sizes lower than 500 nm, and it is observed a variation in size with the N/P ratio parameter. The morphology exhibited by the developed carrier is suitable for cellular uptake /internalization mechanisms, since it has been previously demonstrated that spherical or oval nanoparticles favour transfection efficiency. Particles with spherical shape had greater cellular uptake when compared with those exhibiting

rod-like morphology. This intriguing phenomenon was related with the time that the cell takes to engulf the different shaped particles. (Gaspar *et al*. 2011)

The mean size, the polydispersity index (P.I.), the surface charge and the pDNA encapsulation efficiency of RALA/pDNA formulations were further researched through Dynamic Light Scattering using a Zetasizer Nano Zs. The values are summarized in Table 3.

Table 3: Mean size, polydispersity index, average zeta potential and pDNA encapsulation efficiency (EE) for RALA/pDNA complexes formulated at several N/P ratios. The values were calculated with the data obtained from three independent measurements (mean ± SD, n = 3).

N/P ratio	Size (nm)	P. I.	Zeta Potential (mV)	EE (%)
1	406 ± 9.2	0.2 ± 0.01	+ 2 ± 0.8	47 ± 3.9
2	331 ± 4.7	0.3 ± 0.01	+ 19 ± 2.7	79 ± 5.0
5	212 ± 6.3	0.1 ± 0.01	+ 31 ± 1.8	91 ± 4.8
10	139 ± 4.9	0.3 ± 0.01	+ 37 ± 0.7	94 ± 4.5
15	117 ± 3.7	0.2 ± 0.01	+ 38 ± 2.8	96 ± 3.6
20	102 ± 3.9	0.2 ± 0.02	+ 40 ± 3.2	98 ± 5.1
50	98 ± 4.2	0.3 ± 0.01	+ 40 ± 1.9	98 ± 2.7

The results confirm that all carriers exhibit a size below 500 nm. Moreover, the size of the particles strongly decreases as N/P ratio increases. For highest ratios, however, the decrease in particle size is less pronounced. From N/P ratio of 2, the size of vectors become more suitable for cell uptake and internalization in practical gene delivery applications, as it has been reported that formulations exhibiting sizes below 200 nm turn easier both the cellular uptake and internalization processes, therefore, contributing for efficient gene transfection. (Pezzoli *et al*. 2017) The analysis of polydispersity index (Table 3) allows to infer that all the vectors are monodisperse. Additionally, all polyplexes presented positive surface charges (Table 3), which indicates that pDNA negative charges were fully neutralized. An increase in zeta potential values was found by incrementing the N/P ratio at which RALA/pDNA complexes were formed. As for the size parameter, for higher N/P ratios this effect is not significant. Positively charged nanoparticles interact favourably with the anionic proteoglycans present at the cell surface, being easily attached to the cell what favours the cellular internalization mechanism. Furthermore, it has been stated that delivery systems presenting zeta potential values equal to or higher than +30 mV are considered strongly cationic, fact that enhances their performance to permeate the negatively charged cellular membranes. (E. McNeil 2011) It must be, however, noted that, beyond the promising physicochemical properties exhibited by RALA/pDNA vectors, the success of gene transfection may greatly vary with cell type. (Liu *et al*. 2016) In addition to the parameters investigated, the monitorization of pDNA encapsulation efficiency is essential to promote an effective therapeutic action. The obtained pDNA EEs, for each particle system, are shown in Table 3. With the exception of the formulations at N/P ratio of 1, p53 was

efficiently encapsulated into the carriers. The EE parameter is directly proportional to N/P ratio, with however small differences detected between the vectors at highest N/P ratios. In particular, the nano-systems prepared at N/P ratios of 20 and 50 showed exactly the same pDNA EE. These results for pDNA encapsulation are in accordance with the pDNA immobilization profile observed by agarose gel electrophoresis, presented in Figure 14.

As there is no significant advantage in the use of nanoparticles at higher ratios than N/P of 10, and as N/P ratio of 1 leads to higher sized particles with low pDNA EE, further experimental studies were performed considering, solely, carriers formulated at N/P ratios of 2, 5 and 10.

4.2. pDNA protection studies

It is fundamental to evaluate the stability of RALA/pDNA complexes into the extracellular compartment and to verify the protection that the system confers to the transgene, as this will significantly affect the success of transfection. Hence, in order to get a deep insight into these issues, protection and stability studies were performed for vectors at N/P ratios of 2, 5 and 10.

First the vectors were incubated with DMEM medium supplemented with 10 % of serum (FBS), for different time periods (0, 1, 4, 6 and 12 h), and electrophoresis was used to monitor the pDNA protection. If any degradation occurs by the nucleases present in this medium, it would lead to small and linear fragments, and this short pDNA sequences would readily diffuse out from the particles. (Costa *et al*. 2014) Figure 18 presents the obtained results.

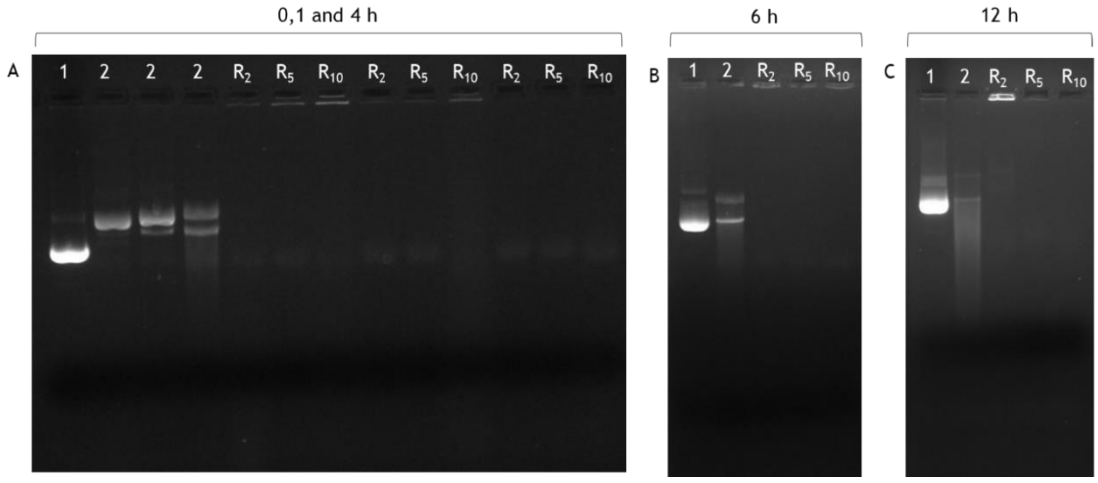

Figure 18: Electrophoretic analysis of the vector's protection of pDNA after its incubation with serum supplemented DMEM + 10 % FBS. The samples were loaded at the application site at the upper end of the image and the lower end is the cathodic end. Image A: incubation of 0, 1 and 4 h - Lane 1: pDNA control; lane 2: non-encapsulated pDNA, 0 h; lane 3: non-encapsulated pDNA, 1 h; lane 4: non-encapsulated pDNA, 4 h; lane 5: RALA/pDNA N/P 2, 0 h; lane 6: RALA/pDNA N/P 5, 0 h; lane 7: RALA/pDNA N/P 10, 0 h; lane 8: RALA/pDNA N/P 2, 1 h; lane 9: RALA/pDNA N/P 5, 1 h; lane 10: RALA/pDNA N/P 10, 1 h; lane 11: RALA/pDNA N/P 2, 4 h; lane 12: RALA/pDNA N/P 5, 4 h; lane 13: RALA/pDNA N/P 10, 4 h. Image B: incubation of 6 h - Lane 14: pDNA control; lane 15: non-encapsulated pDNA; lane 16: RALA/pDNA N/P 2;

lane 17: RALA/pDNA N/P 5; lane 18: RALA/pDNA N/P 10. Image C: incubation of 12 h - lane 19: pDNA control; lane 20: non-encapsulated pDNA; lane 21: RALA/pDNA N/P 2; lane 22: RALA/pDNA N/P 5; lane 23: RALA/pDNA N/P 10.

The data show gradually degradation of non-encapsulated pDNA (naked pDNA) over the incubation time. At 0 h (line 2) pDNA conformation already changed from sc isoform into open circular isoform. During the incubation of 1 to 6 h, the pDNA conformation changes to linear isoform (line 3, 4 e 15) appearing totally degraded at the end of 12 h of incubation (line 20) as evidenced by the band entrapment. However, when pDNA is encapsulated by the developed carrier is seemed to be protected against serum degradation. Nanoparticles are able to ensure protection of the transgene, at least for a 12 h period of serum incubation. This result is in accordance with the obtained result of RALA-FKBPL complexes prepared at N/P ratio 10 exposed to 10 % FCS serum for 4 h. The stability study proved that complexes were stable alone in serum. (Bennett *et al*. 2015)

It is known that DNA can be degraded by DNases, an endonuclease enzyme that catalyses the hydrolytic cleavage of phosphodiester linkages in the DNA backbone, existing in human tissues and serum. (Martinez-Negro *et al*. 2018) For instance, it is important to evaluate the ability of the RALA-based gene vector to protect the plasmid against nucleases. Following this, the different nanoparticles were incubated with DNase I for 1 h and, in another experiment, with DNase I + 10 % SDS, to promote the de-complexation of pDNA from the vectors and observe eventual conformation alteration post assay. The results are shown in Figure 19.

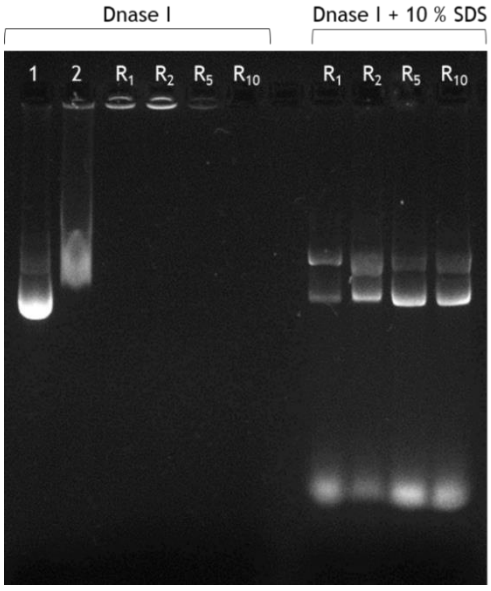

Figure 19: Electrophoretic analysis of the vector's protection of pDNA after its incubation with DNase I and DNase I + 10 % SDS for 1 h. The samples were loaded at the application site at the upper end of the image and the lower end is the cathodic end. Lane 1: pDNA control; lane 2: non-encapsulated pDNA; lane 3: RALA/pDNA N/P 1; lane 4: RALA/pDNA N/P 2; lane 5: RALA/pDNA N/P 5; lane 6: RALA/pDNA N/P 10; lane 8: RALA/pDNA N/P 1; lane 9: RALA/pDNA N/P 2; lane 10: RALA/pDNA N/P 5; lane 11: RALA/pDNA N/P 10.

The study with nucleases confirms the protection ability of the conceived delivery system, since pDNA seems to remain encapsulated into the carriers and do not suffer any degradation from the DNase action. Contrariwise, non-encapsulated pDNA was very degraded when exposed 1 h to this enzyme. Moreover, the assay in the presence of SDS evidences that pDNA is able to keep its integrity and supercoiled isoform after being released from the complexes. The pDNA supercoiled isoform is the most bioactive and the one that promotes higher levels of p53 gene expression. (Venere *et al*. 2018)

Trypsin is a protease belonging to the serine protease family present in human gastric juice of stomach. (Liu *et al*. 2015) The analysis of nanoparticles degradation through the action of trypsin is summarized in Figure 20.

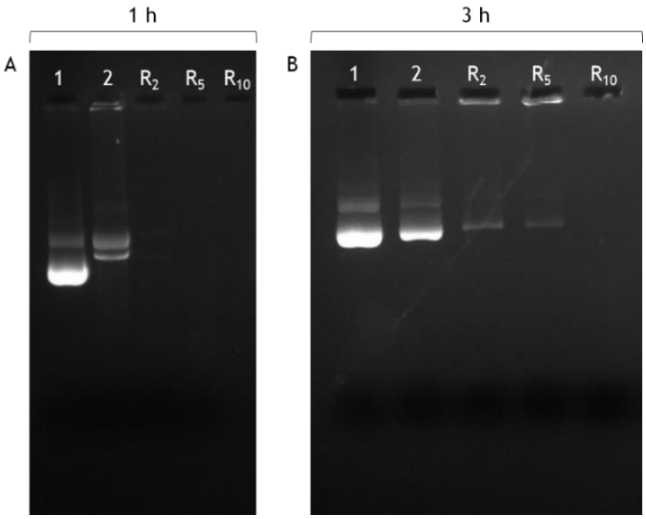

Figure 20: Electrophoretic analysis of the vector's protection of pDNA after its incubation with trypsin. The samples were loaded at the application site at the upper end of the image and the lower end is the cathodic end. Image A: incubation of1 h - Lane 1: pDNA control; lane 2: non-encapsulated pDNA; lane 3: RALA/pDNA N/P 2; lane 4: RALA/pDNA N/P 5; lane 5: RALA/pDNA N/P 10. Image B: incubation of 3 h - lane 1: pDNA control; lane 2: non-encapsulated pDNA; lane 3: RALA/pDNA N/P 2; lane 4: RALA/pDNA N/P 5; lane 5: RALA/pDNA N/P 10.

Images show that nanoparticles integrity was not compromised by incubation with trypsin in the first hour, as evidenced by the absence of pDNA bands in electrophoresis image. However, after 3 h of incubation some pDNA decomplexation from the particles appears to occur for systems at N/P ratios of 2 and 5, as evidenced by the migration of pDNA down the gel. Non-encapsulated pDNA seems to suffer some degradation when exposed to the enzyme.

Finally, the vectors were exposed to 10 % FBS (Figure 21).

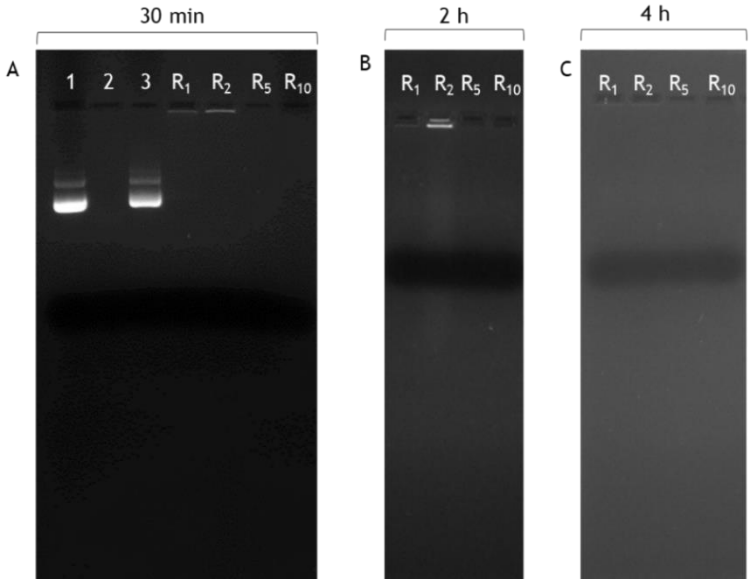

Figure 21: Electrophoretic analysis of the vector's protection of pDNA after its incubation with 10 % FBS. The samples were loaded at the application site at the upper end of the image and the lower end is the cathodic end. Image A: incubation of 30 min - Lane 1: pDNA control; lane 2: 10 % FBS; lane 3: non-encapsulated pDNA; lane 4: RALA/pDNA N/P 1; lane 5: RALA/pDNA N/P 2; lane 6: RALA/pDNA N/P 5; lane 7: RALA/pDNA N/P 10. Image B: incubation of 2 h - Lane 1: RALA/pDNA N/P 1; lane 2: RALA/pDNA N/P 2; lane 3: RALA/pDNA N/P 5; lane 4: RALA/pDNA N/P 10. Image C: incubation of 4 h - Lane 1: RALA/pDNA N/P 1; lane 2: RALA/pDNA N/P 2; lane 3: RALA/pDNA N/P 5; lane 4: RALA/pDNA N/P 10.

Nanoparticles integrity was not compromised during 4 h of incubation as evidenced by the absence of DNA migration down the agarose gel. This reinforces the fact that pDNA is really incorporated in the complexes and that the vectors could remain intact in the presence of simulated biological fluids. Two studies where RALA/pCMV-Luc nanoparticles (McCaffrey *et al.* 2016) and RALA/pDNA polyplexes (McCarthy *et al.* 2014) prepared at N/P ratio 10 were incubated in 10 % FBS revealed that their integrity was not affected and that the complexes remained intact compared to the control pDNA. This agrees with the results presented above.

All these studies demonstrate that, in general, the RALA/pDNA carriers were not adversely affected or degraded by the presence of serum proteins and enzymes, unlike the 'naked' DNA. Moreover, the N/P ratio seems to influence the pDNA degradation behaviour, as a higher N/P ratio leads to more stable particles, preventing the pDNA degradation. Overall, the condensation of pDNA by RALA originate complexes that offer protection and stability to the pDNA against degradation, a requirement that is critical for nucleic acid delivery vehicles *in vivo*.

4.3. Cytotoxicity analysis

Cellular cytotoxicity is a relevant subject to investigate when considering a delivery system for gene transfection applications. Toxicity can compromise the use of delivery systems in gene therapy protocols. This property can be alleviated with cationic peptides that have a low-

molecular weight (≤ 30 residues) and interspersed charged amino acids that are localized on the structure. The RALA cationic peptide contains 7 arginine residues and is within the ideal range of 6–12 arginine residues to reduce toxicity while maintaining critical membrane penetrating potential. (Bennett *et al*. 2015)

To determine the biocompatibility of the developed carriers, MTT assay was performed on fibroblasts cells for 24 and 48 h. Fibroblasts have been chosen to evaluate the cytotoxicity of the nanosystems, due to their normal p53 protein levels. Being non-cancerous cells, any influence on viability profile can be attributed to the incubation with the formulated RALA/pDNA nanoparticles, and this study allows to unravel unequivocally their biocompatibility profile. Contrary, cancer cells present low p53 levels and the incubation with the p53 based systems is expected to lead to p53 gene supplementation what results in the re-establishment of protein levels, and therefore, into a possible therapeutic effect with decrease of cancer cell viability. This fact has been observed in the current work and it will be discussed later. The results on fibroblasts cells, at 24 and 48 h, for several vectors are summarized in Figure 22.

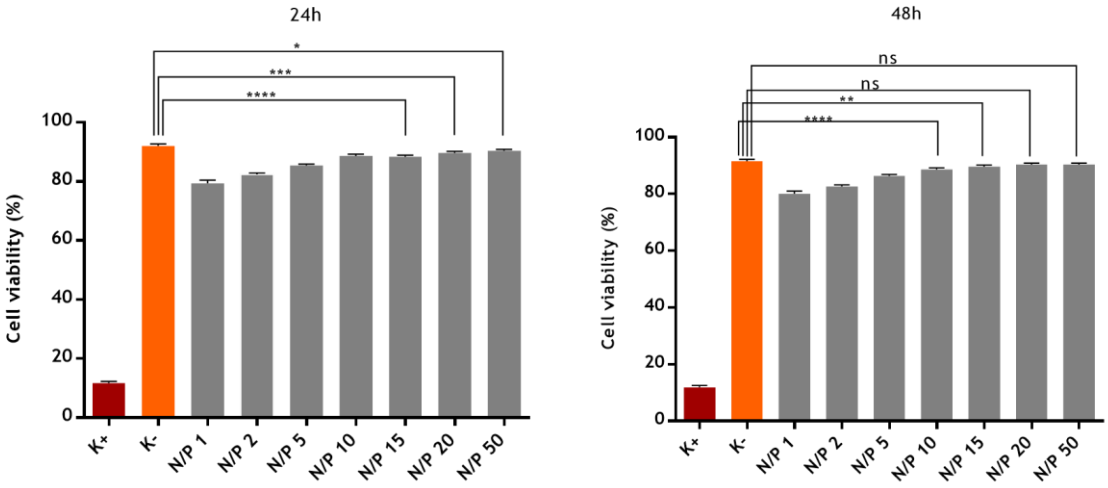

Figure 22: Cellular viability of fibroblast cells after 24 h or 48 h of transfection with RALA/pDNA nanoparticles at various N/P ratios. Percent viability is expressed relative to control cells. The values were calculated with the data obtained from three independent measurements (mean ± SD, n = 3). Non-transfected cells were used as negative control (K^-) and ethanol treated cells were used as positive control (K^+). Statistical analysis was performed using "one-way ANOVA". (ns = $p > 0.05$; **** $p \leq 0.0001$; *** $p \leq 0.001$; ** $p \leq 0.01$; * $p \leq 0.05$)

As can be observed, none of the nanoparticles are toxic to the cells and, thus, it is not expected that they induce an immune or inflammatory response. However, some differences were observed in the cell viability profile between the systems, related to N/P ratio. Results showed that a more biocompatible formulation can be produced by increasing N/P ratio, as fibroblasts viability slightly increases with this parameter (mainly between N/P ratio of 2, 5 and 10). The higher content of amine groups present in RALA peptide seems to contribute to the exhibited

biocompatibility. Similar results were found in other biocompatibility studies with RALA systems. (McCarthy *et al*. 2014) After 48 h incubation with the nanoparticles, the same trend was found (Figure 22).

4.4. Cellular uptake and intracellular location of complexes

The main aim of gene therapy is the efficient delivery of a therapeutic gene into the desired cells, with the ultimate goal of functional protein expression. (Costa *et al*. 2015)

Having established that RALA/pDNA complexes at N/P ratios of 2, 5 and 10 have a set of appropriate characteristics for gene release studies, the mechanisms of cellular uptake and internalization and thus transfection efficacy of nano-systems were evaluated in HeLa cells (a cervical cancer cell line) by Fluorescence Microscopy. Nuclei was stained blue with DAPI and pDNA was green labelled by FITC. The microscopic images obtained from immunohistochemistry of HeLa cells transfected with different carriers after 2 (Figure 23), 4 (Figure 24) and 6 h (Figure 25) are presented below.

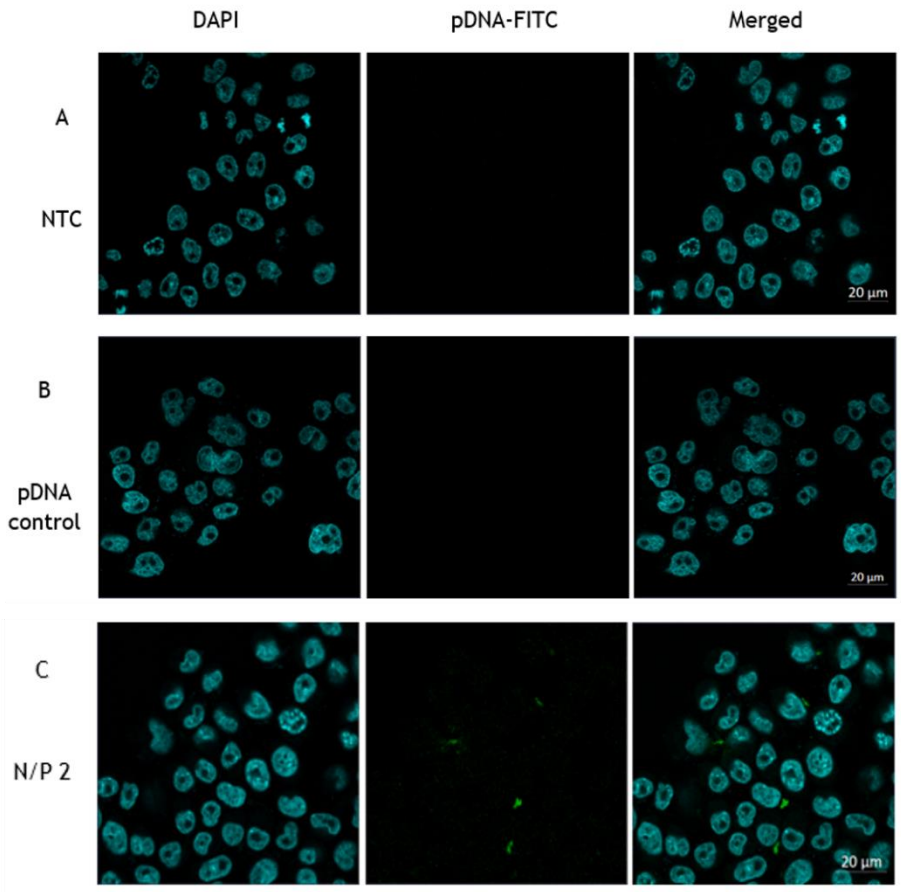

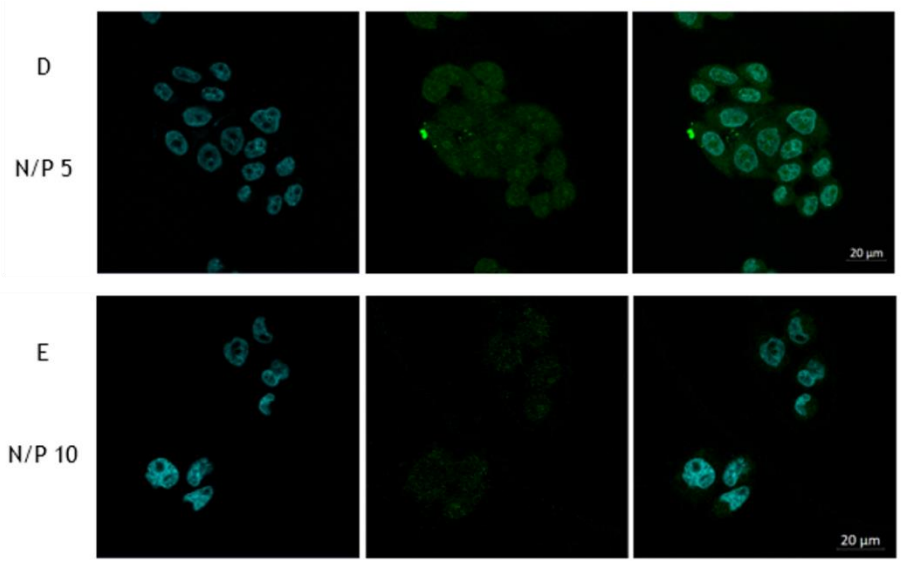

Figure 23: RALA/pDNA vectors transfection ability and intracellular co-localization investigated by fluorescence confocal microscopy after 2 h of transfection. Nucleus is stained blue with DAPI and green represents the pDNA stained with FITC. Representative images of HeLa cells: non-transfected cells (A); HeLa cells after transfection mediated by naked pDNA (B) and RALA/pDNA systems at N/P ratio of 2 (C); 5 (D) and 10 (E). Scale bar = 20 µm.

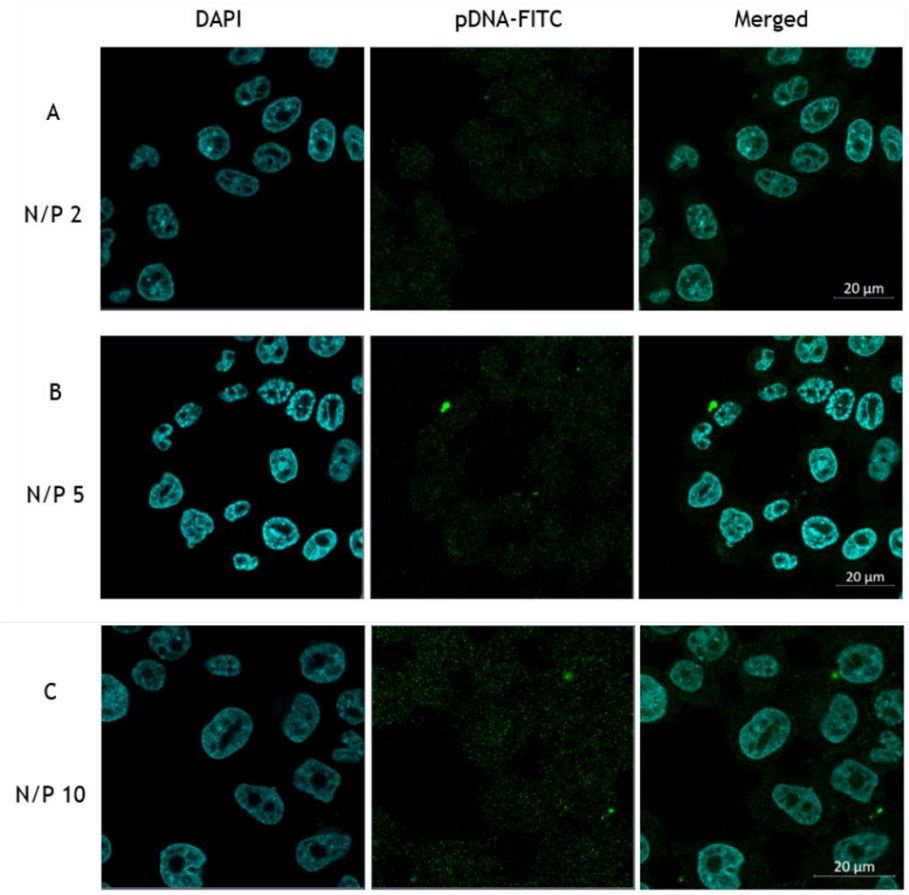

Figure 24: RALA/pDNA vectors transfection ability and intracellular co-localization investigated by fluorescence confocal microscopy after 4 h of transfection. Nucleus is stained blue with DAPI and green

represents the pDNA stained with FITC. Representative images of HeLa cells: HeLa cells after transfection mediated by RALA/pDNA systems at N/P ratio of 2 (A); 5 (B) and 10 (C). Scale bar = 20 µm.

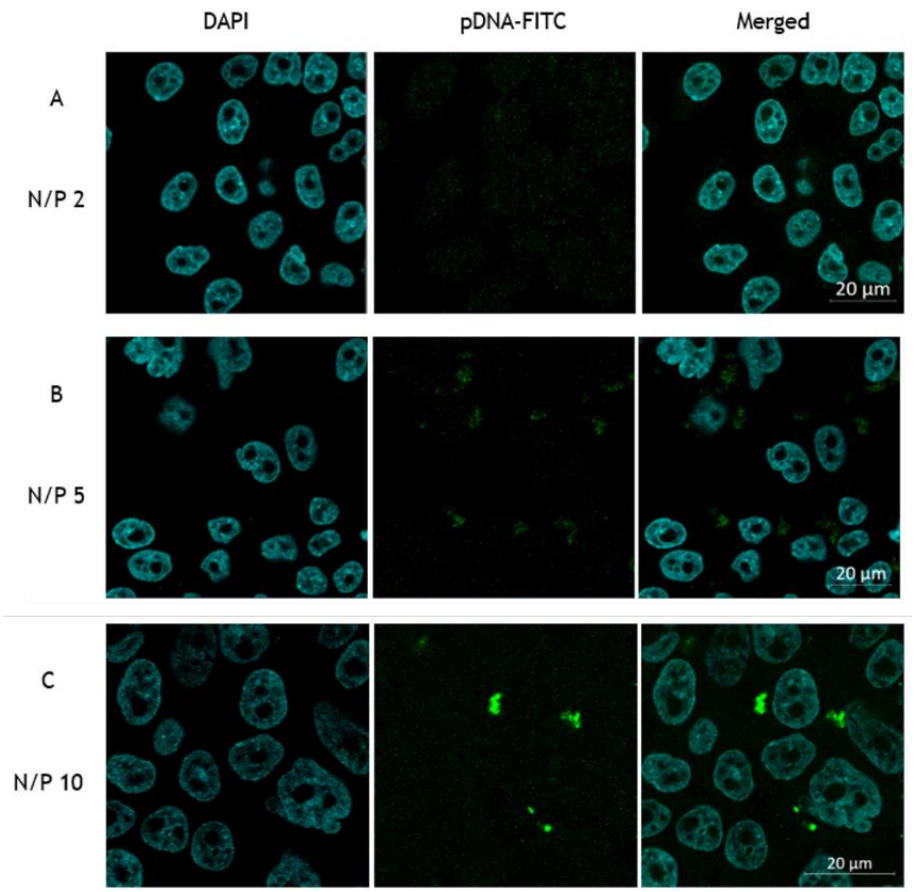

Figure 25: RALA/pDNA vectors transfection ability and intracellular co-localization investigated by fluorescence confocal microscopy after 6 h of transfection. Nucleus is stained blue with DAPI and green represents the pDNA stained with FITC. Representative images of HeLa cells: HeLa cells after transfection mediated by RALA/pDNA systems at N/P ratio of 2 (A); 5 (B) and 10 (C). Scale bar = 20 µm.

Figure 23A from non-transfected cells (control) shows that cells do not exhibit green fluorescence signals. Also, in figure 21B from HeLa cells after 2 h of transfection with naked plasmid (pDNA control) is not observed green fluorescence, probably because the plasmid has a poor cell membrane penetration due to its negative charge and large hydrodynamic size. It may also be easily degraded by serum nucleases present in the medium containing 10 % of serum (FBS) outside the cells, as it was observed in previous stability studies (Figure 21), or digested by enzymes inside the cells into small fragments which are easily 'wash out' from the cell.

Figure 23 (C, D, E) and 24-25 (A, B, C), corresponding to the transfection mediated by RALA-pDNA carriers at 2, 4 and 6 h of transfection, respectively, show the presence of stained pDNA into the tumoral cells. Moreover, the extent of internalization seems to be strongly dependent on the N/P ratio considered. For formulations conceived at N/P ratio of 2 (Figure 23C, 24A and 25A), the green fluorescent dots from pDNA are very weak. This seems to indicate a poor ability for cell uptake, internalization, and consequently, gene transfection. Contrary, vectors

developed at N/P ratios of 5 and 10 are internalized at a higher extent. As discussed above, the properties displayed by these systems, such as their low size, positively charged surface and higher pDNA encapsulation capacity, can strongly promote their cell entry, internalization and pDNA accumulation. The colocalization analysis demonstrates the location of these vehicles, mainly, into the cell nucleus. However, it should be considered the possibility of some carriers being located into the cytoplasmic compartment and perinuclear space.

To further evaluate the effectiveness of RALA/pDNA particles for p53 delivery into HeLa cells, live cell imaging experiments were performed with live HeLa cells as a first approximation of the nanoparticle's penetration capacity. In this type of experiments, the fluorescence of the nanoparticles was tracked over a certain time (each 2 h), to determine if nanoparticles are penetrating cells at specific time and to follow the entry to the nucleus. (Feiner-Gracia *et al*. 2018) Orthogonal sectioning (to construct XZ and YZ images to correspond to an area of interest in an XY image following collection of a z stack of images) was used to determine the cellular localization of fluorescent pDNA at 4 h of transfection. The next three figures illustrate the intracellular distribution of vectors at N/P ratio of 2 (Figure 26), 5 (Figure 27) and 10 (Figure 28), after transfection of HeLa cells for a period of 2, 4 and 6 h.

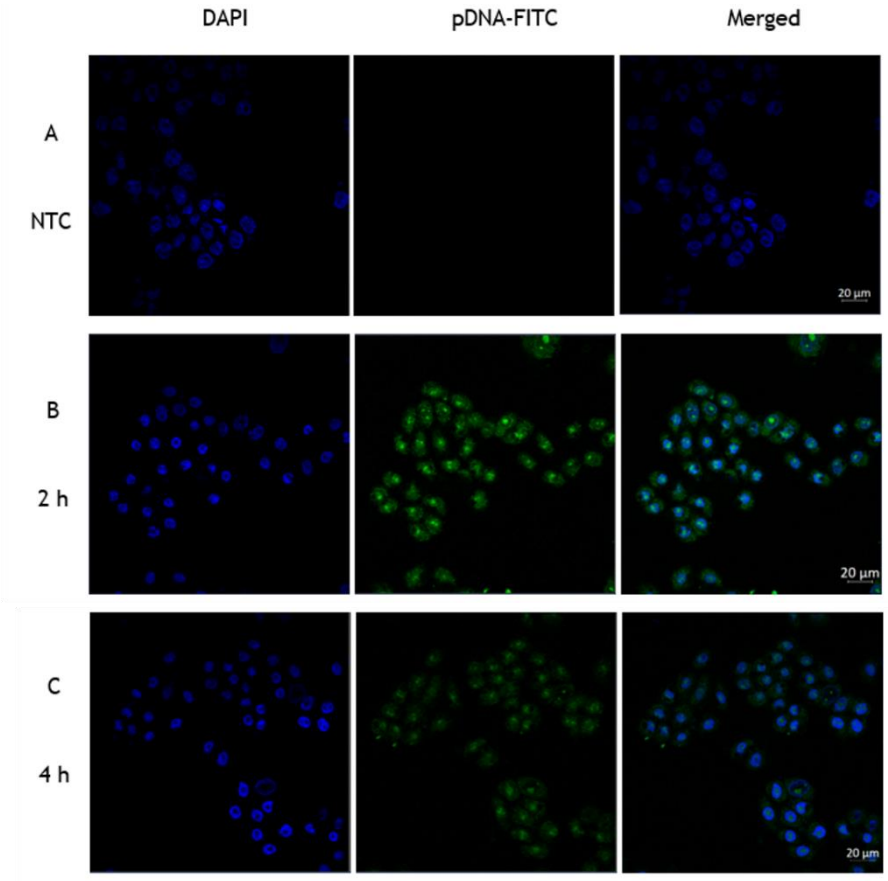

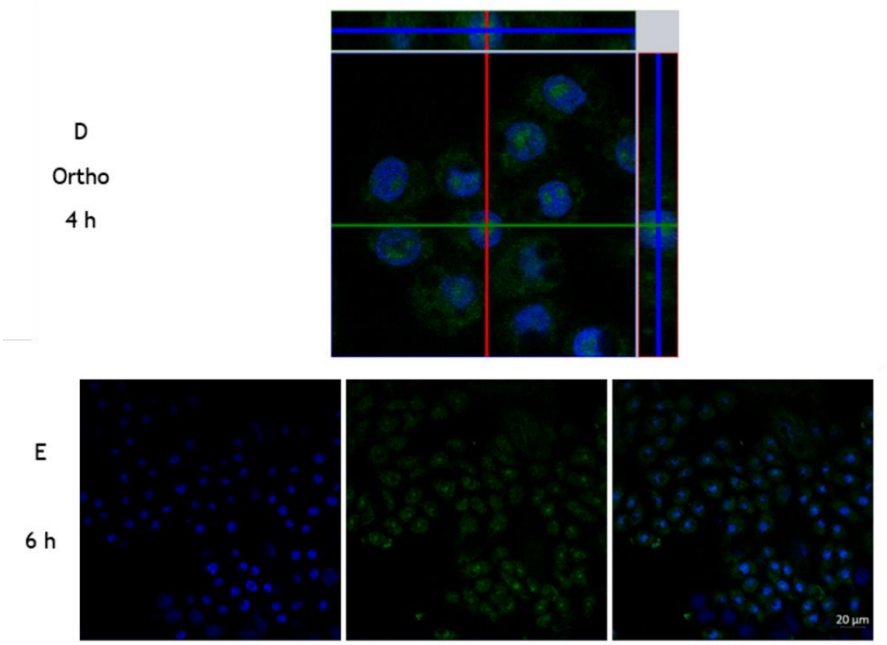

Figure 26: Representative live cell images of the transfection mediated by RALA/pDNA nanoparticles at N/P ratio of 2: non-transfected cells (A) and HeLa cells after 2 h (B); 4 h (C); 4 h, orthogonal view, (D) and 6 h (E). Scale bar = 20 µm.

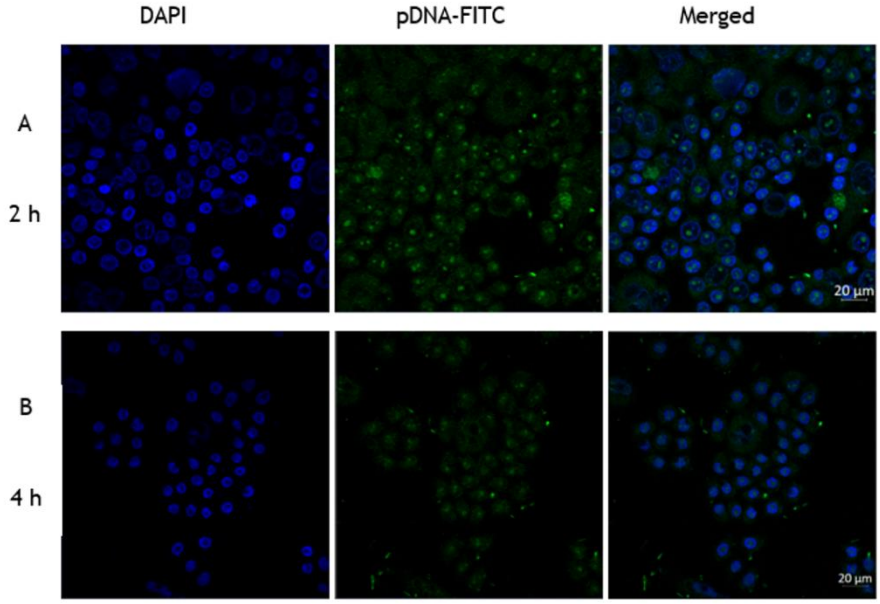

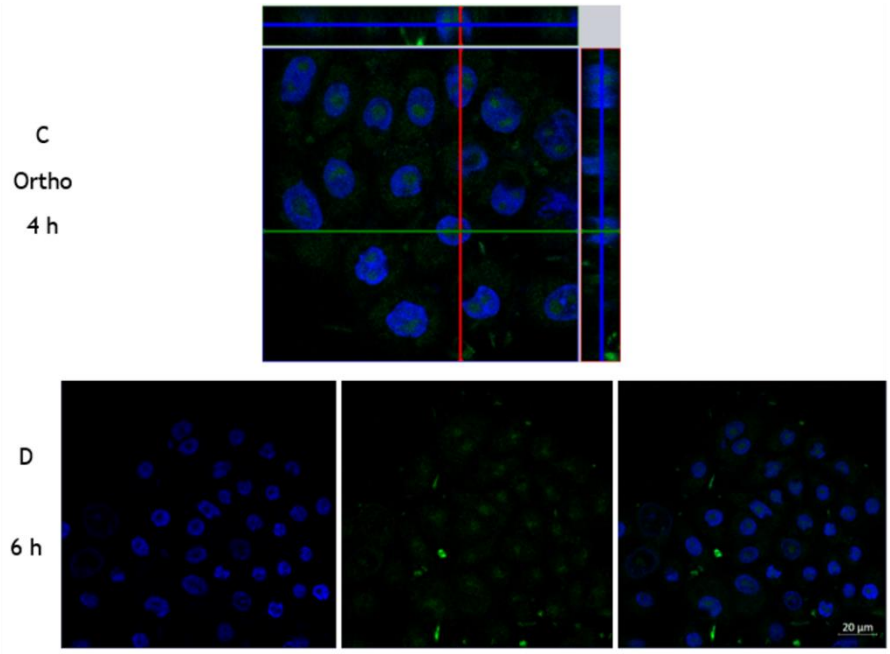

Figure 27: Representative live cell images of the transfection mediated by RALA/pDNA nanoparticles at N/P ratio of 5: HeLa control cells (A) and HeLa cells after 2 h (B); 4 h (C); 4 h, orthogonal view, (D) and 6 h (E). Scale bar = 20 µm.

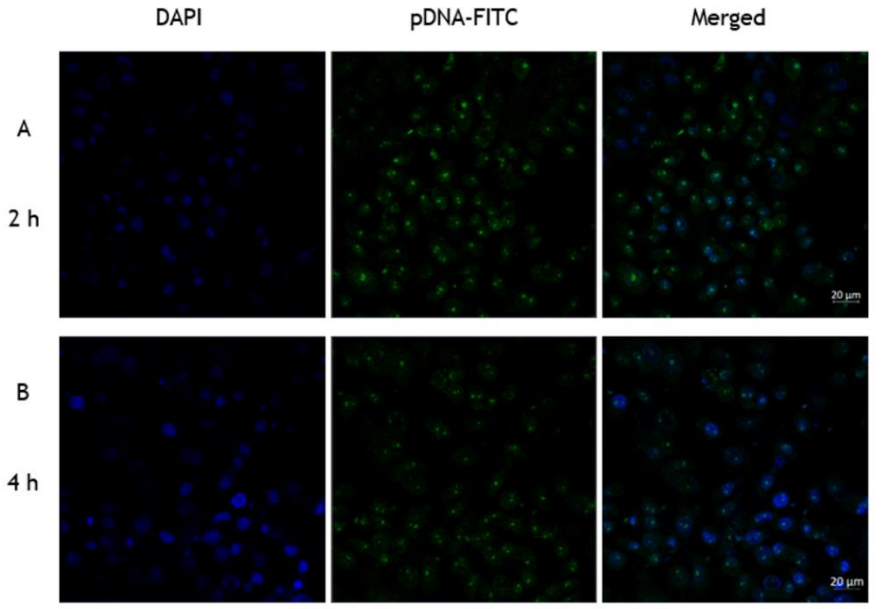

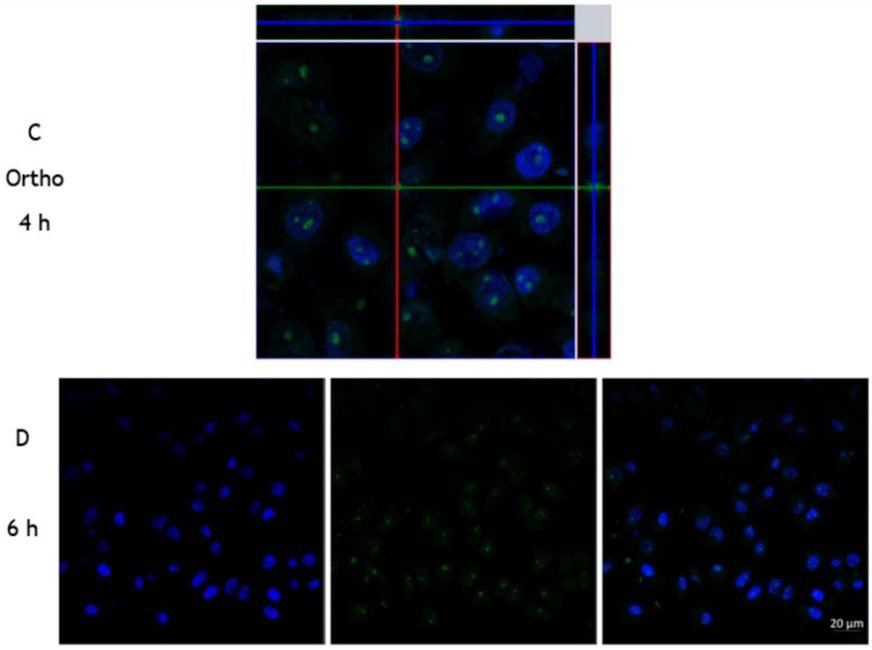

Figure 28: Representative live cell images of the transfection mediated by RALA/pDNA nanoparticles at N/P ratio of 10: HeLa control cells (A) and HeLa cells after 2 h (B); 4 h (C); 4 h, orthogonal view, (D) and 6 h (E). Scale bar = 20 µm.

These nanoparticles were able of cellular internalization and accumulate into the nucleus of cancer cells, already at 2 h (Figure 26B, 27A and 28A). As time proceeds, more pDNA was internalized and accumulated into the nucleus. In addition, the orthogonal view of HeLa cells 4 h after transfection with RALA/pDNA system confirmed the presence of stained pDNA into the nucleus. Furthermore, it is not evident that a longer time of transfection, 6 h, means that the vehicles are internalized into a higher extent. The fluorescence images seem to indicate that the degree of carrier's internalization is comparable at 4 and 6 h of transfection.

The microscopy study reveals, unequivocally, that the nanosystems, at N/P ratios of 5 and 10, are able to overcome both extracellular and intracellular barriers transporting the genetic content to the cytoplasm, possibly, followed by the nuclear trafficking to the nuclear periphery. (Lam and Dean 2010) This mechanism is, apparently, controlled by microtubules; the genetic content is then transported into the nucleus by the cell endogenous import machinery, where the gene of interest can be expressed. (Teo *et al*. 2016) Due to their different properties, the kinetics of gene expression can, however, be different among the developed carriers. Following this achievement, subsequent p53 gene expression is expected when using these vehicles for pDNA delivery into cancer cells.

4.5. p53 gene and protein expression

After transfection of HeLa cells by the developed delivery systems, p53 mRNA expression in transfected cells was detected by RT-PCR assay, using p53 specific primers. Untreated cells were used as control. The results are presented in Figure 29.

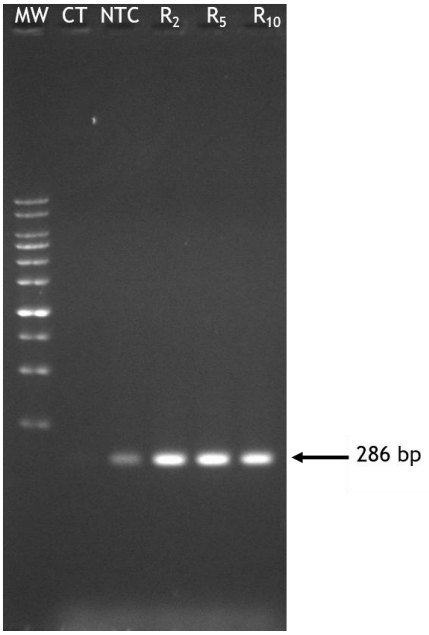

Figure 29: PCR analysis of p53 mRNA in HeLa cells after 24 h of transfection mediated by RALA/pDNA nanoparticles prepared at N/P ratios of 2, 5 and 10. Lane 1: DNA molecular weight marker; lane 2: control without cDNA sample; lane 3 = non-transfected cells; lane 4: cells transfected by RALA/pDNA ratio N/P 2; lane 5: cells transfected by RALA/pDNA ratio N/P 5; lane 6: cells transfected by RALA/pDNA ratio N/P 10.

Considerable levels of p53 mRNA were observed for all RALA/pDNA vectors comparatively to the mRNA content detected in control cells (non-transfected cells). Intense bands from p53 transcripts were found for all RALA/pDNA vectors, demonstrating that all systems seem to promote efficient gene expression. The band intensities are comparable among the three samples (Figure 29).

In order to determine the p53 expression induced by the developed carriers in tumoral cells, western blot analysis was performed. As evidenced in Figure 30, p53 protein seems to be produced for all carriers, although in a different extent. Nanoparticles at N/P ratios of 5 and 10 present more intense bands, to what may correspond higher levels of expressed protein. Although control cells (non-transfected cells) present normal mRNA levels (Figure 29), no protein was detected by western blot. This result observed in control cells can be justified by the fact that most cervical cancers contain wild type p53, however, in most of the cases, p53 protein cannot be detected due to its degradation by HPV oncoproteins. Researchers deeply investigated this subject and found out an interesting relationship between E6 protein of the

oncogenic mucosal-specific HPV types and p53. (Scheffner *et al*. 1993; Thomas, Pim, and Banks 1999) It is currently accepted that E6 protein complexes with p53 leading to its rapid proteasome-mediated degradation through a process involving a set of enzymes: E1 ubiquitin-activating enzyme, E2 ubiquitin-conjugating enzyme, E3 ubiquitin-protein ligase and the complex E6-AP responsible for the ubiquitination of p53 and its subsequent degradation by the proteasome complex 26S. (Thomas, Pim, and Banks 1999) By this reason, the present work intends to supplement the p53 levels in cervical cancer cells, by delivery of a pDNA encoding p53 gene based on peptides nano-systems, to induce cancer cell apoptosis.

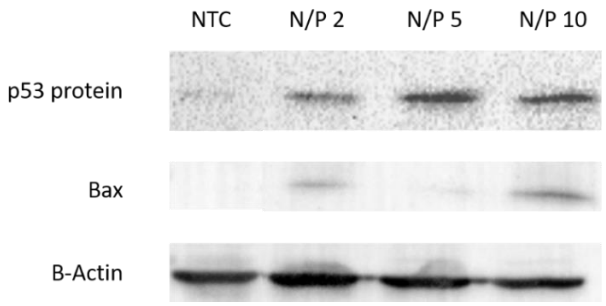

Figure 30: Evaluation of p53 and BAX protein expression by western blot analysis after 48 h transfection with RALA/pDNA nanoparticles prepared at N/P ratios of 2, 5 and 10. Equal amounts of protein (50 ug) were used to detect the expression levels of p53 and BAX. Untreated cells (NTC) were shown as control. B-Actin = 42 kDa; p53 protein = 53 kDa and BAX = 20 kDa.

The results on p53 protein expression were further confirmed by ELISA assay. Table 4 presents the obtained p53 levels in HeLa cells following transfection with naked pDNA and the various RALA/pDNA formulations.

Table 4: Quantification of p53 protein levels in HeLa cells after 24 h of transfection mediated by the formulated RALA/pDNA systems formulated at N/P ratios of 2, 5 and 10. The values were calculated with the data obtained from three independent measurements (mean $\pm$ SD, n = 3).

System	p53 content/(ng/mL)
Control cells (non-transfected)	0
Naked pDNA	0
RALA/pDNA N/P 2	120 $\pm$ 6.6
RALA/pDNA N/P 5	465 $\pm$ 4.2
RALA/pDNA N/P 10	482 $\pm$ 5.8

As it is presented in Table 4, p53 protein was not detected when transfection was mediated by naked pDNA, what reinforces the need for pDNA encapsulation into a delivery system in order to ensure the protection and stability of the transgene, thus, guaranteeing the success of transfection process. Different protein content can be produced depending on the N/P ratio considered. Vectors at N/P ratio of 2 present the lowest p53 amount, while as N/P ratio increases higher p53 levels can be quantified in cancer cells. The effect on p53 expression of

increasing the N/P ratio from 5 to 10 is, however, quite small indicating that a plateau on transfection efficiency is perhaps reached at N/P ratio of 5. Therefore, these results seem to prove that beyond N/P ratio of 5, there is no significant advantage in the increment of peptide amount into the complexes. This observation correlates well with the observed fluorescence images for the cell entry phenomenon, where a dramatic difference is observed between vectors at N/P ratios of 2 and 5 or 2 and 10, but not between carriers at N/P ratios of 5 and 10. These data demonstrates that the transgene expression promoted by the highest N/P ratios RALA/pDNA vectors can lead to considerable p53 protein levels in HeLa cells, suggesting that these formulations may represent a powerful and valuable tool for p53 based cancer therapy.

4.6. Vector-mediated apoptosis

4.6.1. Caspase-3 activity assay

Apoptosis is a complex physiological process responsible for the maintenance of normal cell function, involving cysteine aspartate specific proteases. (Baig *et al.* 2016; Pfeffer and Singh 2018) Initiator caspases (2, 8 and 10) and execution caspases (3, 6 and 7) are the effector molecules of this cell death mechanism by two main pathways. Both extrinsic and intrinsic pathways lead to a cascade of molecular events that culminate into the activation of caspase 3. (Pfeffer and Singh 2018) Therefore, assaying for caspase-3 activity allows apoptosis detection. Information on apoptosis in HeLa cells by the action of RALA/pDNA vectors was first assessed by measuring caspase-3 activity (Figure 31).

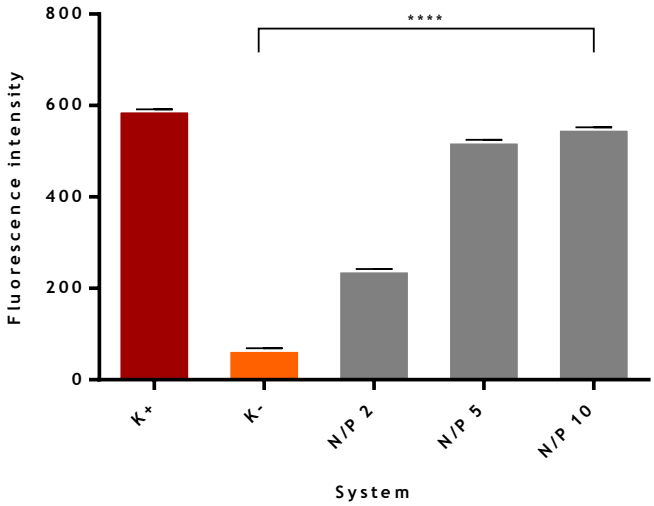

Figure 31: Caspase-3 activity in HeLa cells after 48 h of transfection mediated by RALA/pDNA vectors at N/P ratios of 2, 5 and 10. Negative control (K-) corresponds to non-transfected HeLa cells while incubation with 1 μM of staurosporine for 48 h was used as positive control (K+). The vectors induced caspase-3 activity relatively to negative control. Statistically significant differences among groups were determined by "one-way ANOVA" (n = 3). (**** $p < 0.0001$)

Figure 31 shows that the transfection mediated by the developed nano-systems leads to the activation of caspase-3 activity and, thus, to apoptosis in HeLa cells. A remarkable difference in the fluorescence intensity was found between carriers conceived at N/P ratio of 2 and the ones at N/P ratios of 5 and 10. The lowest N/P ratio vectors lead to lower caspase-3 activation activity to what may also indicate a lower extent of apoptosis in cancer cells. The difference between the two highest N/P ratios is very small, with transfection using nanoparticles at N/P ratio of 10 promoting slightly higher fluorescence intensity.

4.6.2. HeLa cells - MTT assay

Additionally, an MTT assay on HeLa cells further supports the evidence of apoptosis. The obtained results are represented in Figure 32.

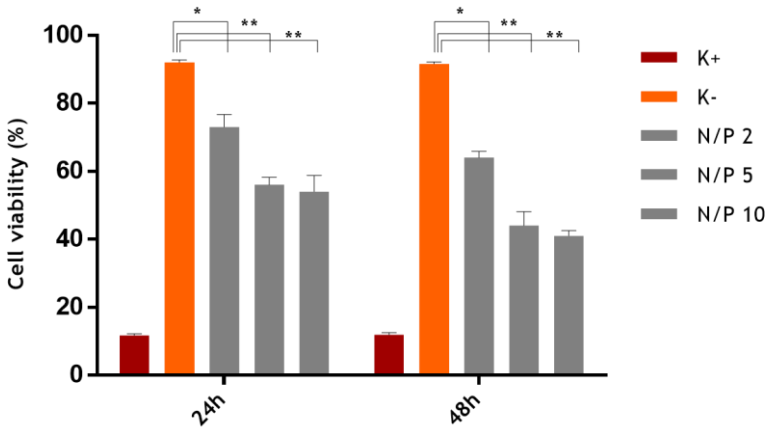

Figure 32: Cell viability of HeLa cells after 24 and 48 h of transfection with RALA/pDNA complexes at different N/P ratios. Non-transfected cells were used as negative control (K-) and ethanol treated cells were used as positive controls (K+) for cytotoxicity. Statistical analysis was made using "one-way ANOVA" with data obtained from three independent measurements (mean ± SD, n = 3) . (** $p \leq 0.01$; * $p \leq 0.05$)

Figure 32 presents a decrease in cellular viability after the incubation of HeLa cells (24 and 48 h) with the considered formulations. The extent of this phenomenon is dependent on the N/P ratio considered; a more significant inhibition of cell growth is achieved with systems prepared at higher N/P ratios and after two days of incubation. These data indicate that the observed cell death can be a signal of apoptosis induced by p53 gene expression mediated by the nano-systems and not a cytotoxic effect promoted by the formulation itself. As demonstrated earlier on this report in a study on fibroblast cells, RALA/pDNA vectors are biocompatible.

4.6.3. TUNEL assay

Cancer cell apoptosis induced by the transfection of RALA/pDNA vectors was investigated by TUNEL method. The key role in the TUNEL assay is played by the endonuclease terminal deoxynucleotidyl transferase (TdT) that catalyses the attachment of a modified analogue of deoxynucleotides (dUTPs) to the free -OH terminus of the DNA strand breaks. These dUTPs are

labelled using various markers that allow for the detection of DNA strand breaks directly. Depending upon the level the visualization will be fluorescent. (Majtnerova and Rousar 2018) This assay gives information on apoptotic cell death by detecting DNA strand breaks. A summary of the performed study is presented in Figure 33.

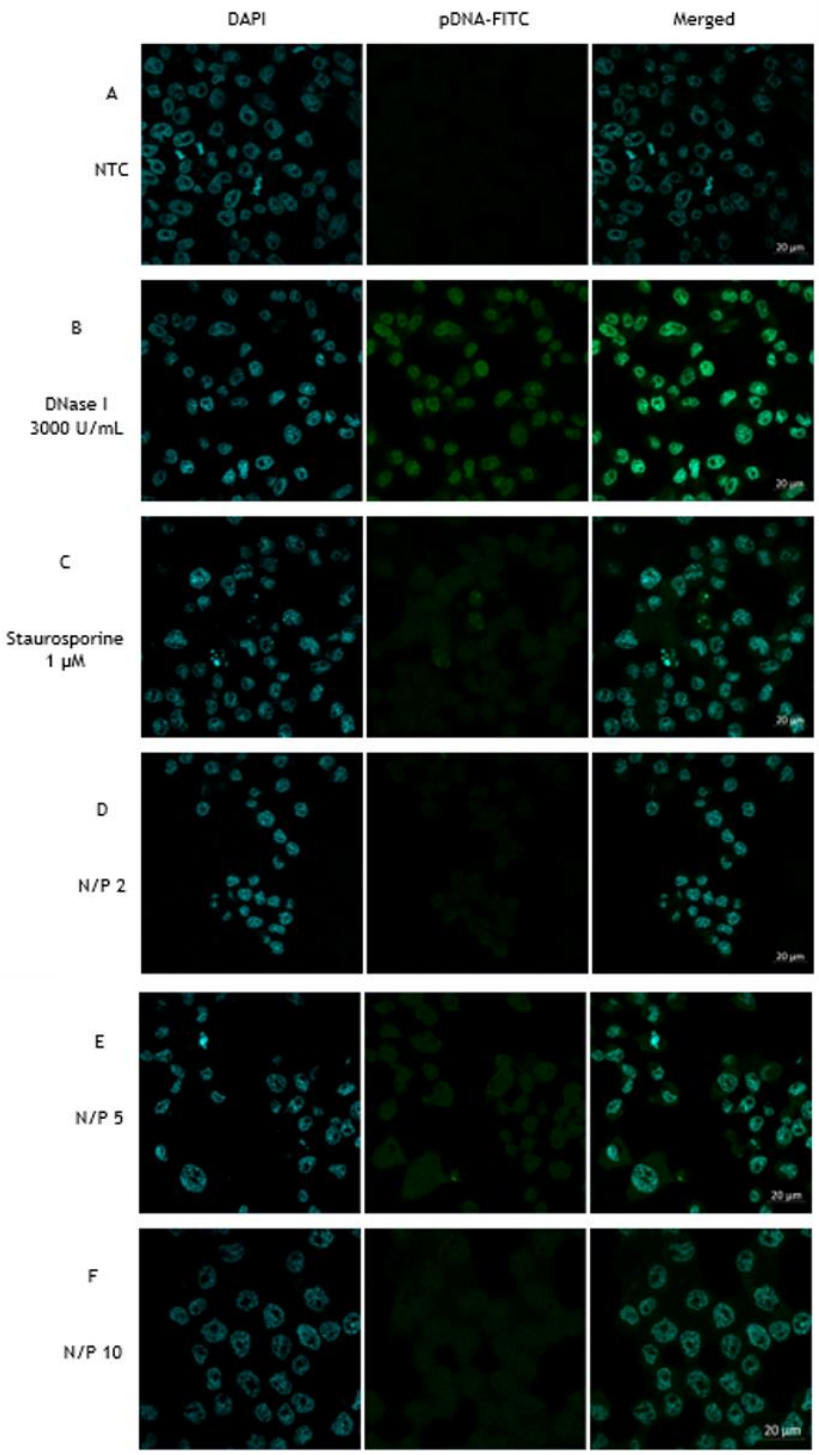

Figure 33: In situ cell death detection in HeLa cells assayed by terminal deoxynucleotidyl transferase-mediated dUTP nick end labelling (TUNEL). Representative images of HeLa cells taken by confocal

microscopy: control cells [non transfected] (A), cells incubated with DNase I for 10 min (manufacturer's recommended positive control) (B), cells incubated for 6 h with staurosporine (positive control) (C) and cells incubated with RALA/pDNA vectors at N/P ratios of 2 (D), 5 (E) and 10 (F). Blue: DAPI nuclear stain. Green: FITC pDNA stain and scale bar = 20 μm.

Through confocal microscopy observation, HeLa cells treated with DNase I and staurosporine (positive controls) showed green staining, which indicated DNA fragmentation. Evidences of apoptosis induction can also be detected in cancer cells when transfection is mediated by the studied RALA/pDNA formulations. These findings agree well with those of DAPI-staining; FITC dye binds to the minor groove of DNA (AT) site emitting fluorescence. (Estandarte *et al*. 2016) HeLa cells treated with RALA/pDNA particles exhibited a FITC-positive phenotype demonstrate DNA nuclear fragmentation. Although it is hard to predict differences between the systems it seems that increasing N/P ratio a more intense green fluorescence staining can be found in HeLa cells. The obtained images suggest that the carriers developed at N/P ratios of 5 and 10 induce cancer cell apoptosis in a large extent. This fact correlates well with the observed higher cellular internalization for these systems, as well as, the higher levels of produced p53.

At this point, the obtained results on Hela cells can be correlate with efficient transfection, effective gene expression and p53 protein supplementation in cancer cells with consequent apoptosis. Other authors found the same phenomenon on HeLa cells when studying p53 based nano-platforms. (Valente *et al*. 2018; Gaspar *et al*. 2011) Altogether, these results on apoptosis agree well with the tendency, already observed, between the different N/P ratio vehicles, which it is consistent with enhanced physicochemical properties, high ability for cell uptake/internalization, higher produced protein levels and large extent of apoptosis for the RALA/pDNA vectors developed at higher N/P ratios.

To get a deeper understanding on the apoptosis mechanism induced by the RALA/pDNA vector, namely information on the apoptotic activated pathway, the BAX protein expression on HeLa cells has been evaluated by western blot analysis. The results for the peptide/pDNA complexes at N/P ratios of 2, 5 and 10 are shown in Figure 30. Image reveals that no BAX was detected for control cells (non-transfected), however it is observed the presence of BAX in cells transfected with nanoparticles. The bands seem to be little intense given that the marking was realised on the same membrane as the used for p53 revelation. The electrotransference time used for this western blot procedure is appropriated for high weight proteins, like p53 and ß-actin proteins, and could not be the most favourable for proteins with less molecular weight, like BAX protein, making difficult the bans detection. However, these results suggest that the BAX protein is produced on cancer cells when transfection has been mediated by these systems. A more intense band seems to appear for N/P ratio of 10 meaning that a slightly higher BAX expression was achieved for this ratio. The increment of BAX protein in HeLa cells transfected with RALA/pDNA nano-systems indicates that apoptosis occurs via the intrinsic pathway, since this

protein is downregulated by the Bcl-2 protein family, as it is depicted in Figure 1 of Introduction section.(Kalkavan and Green 2018)

Unexpectedly, a less intense band from BAX expression can be observed for nanoparticles at N/P ratio of 5. Considering the evidences of a similar transfection efficiency and apoptosis induction for particles at N/P ratios of 5 and 10, already documented in this thesis, it would be expected that at N/P ratio of 5, this protein would be expressed. However, from BAX results it was not possible to observe the same behaviour. This may be due to some experimental failure at the western assay. This method involves numerous sensible steps and a change in one parameter during the procedure could have compromised the result. This is still an ongoing work and special attention is being devoted to the optimization of experimental procedure in order to get more accurate results on BAX expression for this ratio.

Chapter V - Conclusions and future perspectives

Cancer is still one of the most deadly and severe diseases humankind has to face. The conventional cancer therapies which include, surgery, radiotherapy and chemotherapy, are commonly ineffective and due to the large number of secondary side effects arising from their application, researchers still seek new approaches when considering cancer treatment. The number of deaths by cancer is increasing in an exponential way worldwide. In particular, cervical cancer is the fourth most frequent cancer in women and novel and innovative therapies are mandatory to control the expansion of the disease, especially on undeveloped countries, as some African countries.

Gene therapy emerged as a potential tool to treat numerous types of cancers and consists in the delivery of DNA to cells to correct a genetic defect or supplement the level of a given biomolecule that is abnormally expressed. For gene therapy to be feasible and viable in a clinical setting, the design and development of a suitable delivery system is needed. Among the broad variety of non-viral carrier materials, cell-penetrating peptides conquered a prominent role due to their structural characteristics, sequence and function.

In this context, RALA peptide/pDNA complexes have been developed at several N/P ratios and revealed to possess a set of properties that strongly vary with this parameter.

The formulated vectors presented ideal characteristics as nanometric sizes, spherical or oval morphology, positive surface charge, good encapsulation efficiency and capacity of resist to serum nucleases that make them suitable for cell uptake and internalization. The fact that the properties of RALA/pDNA vectors can be controlled by N/P ratio opens the possibility of engineering tunable RALA/pDNA systems to optimize their characteristics, increasing their performance as delivery vehicles. *In vitro* studies on fibroblasts cells revealed the systems biocompatibility and studies on HeLa cells showed that the great characteristics of RALA/pDNA polyplexes contributed to overcome the intracellular barriers, be internalized and then co-localized in the nucleus. This capacity resulted in effective p53 gene delivery and further mRNA transcripts and protein expression, in an extent dependent on the ratio used. The apoptosis assays indicated that the delivery of plasmid DNA and consequent production of p53 protein induced cancer cell death. Our collective approach brings significant improvements on the application of cell penetrating peptides in the development of tailored and high-performance p53 gene-based platforms for translational cancer therapy.

Ongoing work on this delivery system is focussed on the apoptosis mechanism and in revealing the activated cell death pathway on cancer HeLa cells when transfection is mediated by RALA/pDNA carriers. Moreover, future directions will include *in vivo* studies, to test the ability of the developed system in supress/inhibit tumour growth and, therefore, cancer development.

Additionally, this work had provided valuable information and knowledge on the potential use of cell penetrating peptides in the design/development of peptide/pDNA based delivery systems for cancer gene therapy applications. Following this, novel peptides are being synthesized for the formulation of innovative carriers that will be deeply explored in a near future. This clearly opens an entire research subject that will, surely, found advanced therapeutic applications in biotechnological, biopharmaceutical and biomedical areas.

Chapter VI - Bibliography

Abdulrahman, Ahmed, and Ashraf Ghanem. 2018. 'Recent advances in chromatographic purification of plasmid DNA for gene therapy and DNA vaccines: A review', *Analytica Chimica Acta*, 1025: 41-57.

Ali, A. A., C. M. McCrudden, J. McCaffrey, J. W. McBride, G. Cole, N. J. Dunne, T. Robson, A. Kissenpfennig, R. F. Donnelly, and H. O. McCarthy. 2017. 'DNA vaccination for cervical cancer; a novel technology platform of RALA mediated gene delivery via polymeric microneedles', *Nanomedicine*, 13: 921-32.

Baig, S., I. Seevasant, J. Mohamad, A. Mukheem, H. Z. Huri, and T. Kamarul. 2016. 'Potential of apoptotic pathway-targeted cancer therapeutic research: Where do we stand?', *Cell Death Dis*, 7: e2058.

Bennett, Rachel, Anita Yakkundi, Hayley D. McKeen, Lana McClements, Thomas J. McKeogh, Cian M. McCrudden, Kenneth Arthur, Tracy Robson, and Helen O. McCarthy. 2015. 'RALA-mediated delivery of FKBPL nucleic acid therapeutics', *Nanomedicine (London, England)*, 10: 2989-3001.

Caffery, Breanne, Jeoung Lee, and Angela Alexander-Bryant. 2019. 'Vectors for Glioblastoma Gene Therapy: Viral & Non-Viral Delivery Strategies', *Nanomaterials*, 9.

Chabeda, A., R. J. R. Yanez, R. Lamprecht, A. E. Meyers, E. P. Rybicki, and Hitzeroth, II. 2018. 'Therapeutic vaccines for high-risk HPV-associated diseases', *Papillomavirus Res*, 5: 46-58.

Chalanqui, M. J., S. Pentlavalli, C. McCrudden, P. Chambers, M. Ziminska, N. Dunne, and H. O. McCarthy. 2019. 'Influence of alginate backbone on efficacy of thermo-responsive alginate-g-P(NIPAAm) hydrogel as a vehicle for sustained and controlled gene delivery', *Mater Sci Eng C Mater Biol Appl*, 95: 409-21.

Chen, C., D. Yue, L. Lei, H. Wang, J. Lu, Y. Zhou, S. Liu, T. Ding, M. Guo, and L. Xu. 2018. 'Promoter-Operating Targeted Expression of Gene Therapy in Cancer: Current Stage and Prospect', *Mol Ther Nucleic Acids*, 11: 508-14.

Costa, D., T. Albuquerque, J. A. Queiroz, and A. J. M. Valente. 2019. 'A co-delivery platform based on plasmid DNA peptide-surfactant complexes: formation, characterization and release behavior', *Colloids Surf B Biointerfaces*, 178: 430-38.

Costa, D., W. H. Briscoe, and J. Queiroz. 2015. 'Polyethylenimine coated plasmid DNA-surfactant complexes as potential gene delivery systems', *Colloids Surf B Biointerfaces*, 133: 156-63.

Costa, Diana, Artur J. M. Valente, M. Graça Miguel, and João Queiroz. 2014. 'Plasmid DNA microgels for drug/gene co-delivery: A promising approach for cancer therapy', *Colloids and Surfaces A: Physicochemical and Engineering Aspects*, 442: 181-90.

Dev, S. B., and Lee Walters. 1990. 'Fourier transform infrared spectroscopy for the characterization of a model peptide–DNA interaction', *Biopolymers*, 29: 289-99.

Diogo, M. M., J. A. Queiroz, G. A. Monteiro, S. A. M. Martins, G. N. M. Ferreira, and D. M. F. Prazeres. 2000. 'Purification of a cystic fibrosis plasmid vector for gene therapy using hydrophobic interaction chromatography', *Biotechnology and Bioengineering*, 68: 576-83.

E. McNeil, Scott. 2011. *Characterization of Nanoparticles Intended for Drug Delivery*.

El-Deeb, N. M., A. M. Yassin, L. A. Al-Madboly, and A. El-Hawiet. 2018. 'A novel purified Lactobacillus acidophilus 20079 exopolysaccharide, LA-EPS-20079, molecularly regulates both apoptotic and NF-kappaB inflammatory pathways in human colon cancer', *Microb Cell Fact*, 17: 29.

Estandarte, A. K., S. Botchway, C. Lynch, M. Yusuf, and I. Robinson. 2016. 'The use of DAPI fluorescence lifetime imaging for investigating chromatin condensation in human chromosomes', *Sci Rep*, 6: 31417.

Feiner-Gracia, N., A. Dols-Perez, M. Royo, C. Solans, M. J. Garcia-Celma, and C. Fornaguera. 2018. 'Cell penetrating peptide grafting of PLGA nanoparticles to enhance cell uptake', *European Polymer Journal*, 108: 429-38.

Fulda, S., and K. M. Debatin. 2006. 'Extrinsic versus intrinsic apoptosis pathways in anticancer chemotherapy', *Oncogene*, 25: 4798-811.

Gaspar, V. M., F. Sousa, J. A. Queiroz, and I. J. Correia. 2011. 'Formulation of chitosan-TPP-pDNA nanocapsules for gene therapy applications', *Nanotechnology*, 22: 015101.

Ghanem, A., R. Healey, and F. G. Adly. 2013. 'Current trends in separation of plasmid DNA vaccines: a review', *Anal Chim Acta*, 760: 1-15.

Grilo, A. L., and A. Mantalaris. 2019. 'Apoptosis: A mammalian cell bioprocessing perspective', *Biotechnol Adv*, 37: 459-75.

Guidotti, G., L. Brambilla, and D. Rossi. 2017. 'Cell-Penetrating Peptides: From Basic Research to Clinics', *Trends Pharmacol Sci*, 38: 406-24.

Hardee, C. L., L. M. Arevalo-Soliz, B. D. Hornstein, and L. Zechiedrich. 2017. 'Advances in Non-Viral DNA Vectors for Gene Therapy', *Genes (Basel)*, 8.

Hoppe-Seyler, K., F. Bossler, J. A. Braun, A. L. Herrmann, and F. Hoppe-Seyler. 2018. 'The HPV E6/E7 Oncogenes: Key Factors for Viral Carcinogenesis and Therapeutic Targets', *Trends Microbiol*, 26: 158-68.

Ikuta, N., A. Tanaka, A. Otsubo, N. Ogawa, H. Yamamoto, T. Mizukami, S. Arai, M. Okuno, K. Terao, and S. Matsugo. 2014. 'Spectroscopic studies of R(+)-alpha-lipoic acid--cyclodextrin complexes', *Int J Mol Sci*, 15: 20469-85.

Jahangirian, H., E. G. Lemraski, T. J. Webster, R. Rafiee-Moghaddam, and Y. Abdollahi. 2017. 'A review of drug delivery systems based on nanotechnology and green chemistry: green nanomedicine', *Int J Nanomedicine*, 12: 2957-78.

Jain, A. K., A. Massey, H. Yusuf, D. M. McDonald, H. O. McCarthy, and V. L. Kett. 2015. 'Development of polymeric-cationic peptide composite nanoparticles, a nanoparticle-in-nanoparticle system for controlled gene delivery', *Int J Nanomedicine*, 10: 7183-96.

Jiang, Y., S. Huo, J. Hardie, X. J. Liang, and V. M. Rotello. 2016. 'Progress and perspective of inorganic nanoparticle-based siRNA delivery systems', *Expert Opin Drug Deliv*, 13: 547-59.

Kalkavan, H., and D. R. Green. 2018. 'MOMP, cell suicide as a BCL-2 family business', *Cell Death Differ*, 25: 46-55.

Kim, J., D. R. Wilson, C. G. Zamboni, and J. J. Green. 2015. 'Targeted polymeric nanoparticles for cancer gene therapy', *J Drug Target*, 23: 627-41.

Konate, K., M. Dussot, G. Aldrian, A. Vaissiere, V. Viguier, I. F. Neira, F. Couillaud, E. Vives, P. Boisguerin, and S. Deshayes. 2019. 'Peptide-Based Nanoparticles to Rapidly and Efficiently "Wrap 'n Roll" siRNA into Cells', *Bioconjug Chem*, 30: 592-603.

Lam, A. P., and D. A. Dean. 2010. 'Progress and prospects: nuclear import of nonviral vectors', *Gene Ther*, 17: 439-47.

Lee, J. H., J. H. Wang, J. Chen, F. Li, T. L. Edwards, A. W. Hewitt, and G. S. Liu. 2019. 'Gene therapy for visual loss: Opportunities and concerns', *Prog Retin Eye Res*, 68: 31-53.

Lembo, D., and R. Cavalli. 2010. 'Nanoparticulate delivery systems for antiviral drugs', *Antivir Chem Chemother*, 21: 53-70.

Liu, C., B. Sun, N. An, W. Tan, L. Cao, X. Luo, Y. Yu, F. Feng, B. Li, M. Wu, C. Su, and X. Jiang. 2011. 'Inhibitory effect of Survivin promoter-regulated oncolytic adenovirus carrying P53 gene against gallbladder cancer', *Mol Oncol*, 5: 545-54.

Liu, M., B. Feng, Y. Shi, C. Su, H. Song, W. Cheng, and L. Zhao. 2015. 'Protamine nanoparticles for improving shRNA-mediated anti-cancer effects', *Nanoscale Res Lett*, 10: 134.

Liu, X., F. Wu, Y. Tian, M. Wu, Q. Zhou, S. Jiang, and Z. Niu. 2016. 'Size Dependent Cellular Uptake of Rod-like Bionanoparticles with Different Aspect Ratios', *Sci Rep*, 6: 24567.

Majtnerova, P., and T. Rousar. 2018. 'An overview of apoptosis assays detecting DNA fragmentation', *Mol Biol Rep*, 45: 1469-78.

Martinez-Negro, M., A. L. Barran-Berdon, C. Aicart-Ramos, M. L. Moya, C. T. de Ilarduya, E. Aicart, and E. Junquera. 2018. 'Transfection of plasmid DNA by nanocarriers containing a gemini cationic lipid with an aromatic spacer or its monomeric counterpart', *Colloids Surf B Biointerfaces*, 161: 519-27.

Massey, Ashley S., Sreekanth Pentlavalli, Richard Cunningham, Cian M. McCrudden, Emma M. McErlean, Philip Redpath, Ahlam A. Ali, Stephanie Annett, John W. McBride, Joanne McCaffrey, Tracy Robson, Marie E. Migaud, and Helen O. McCarthy. 2016. 'Potentiating the Anticancer Properties of Bisphosphonates by Nanocomplexation with the Cationic Amphipathic Peptide, RALA', *Molecular Pharmaceutics*, 13: 1217-28.

McCaffrey, J., C. M. McCrudden, A. A. Ali, A. S. Massey, J. W. McBride, M. T. McCrudden, E. M. Vicente-Perez, J. A. Coulter, T. Robson, R. F. Donnelly, and H. O. McCarthy. 2016. 'Transcending epithelial and intracellular biological barriers; a prototype DNA delivery device', *J Control Release*, 226: 238-47.

McCarthy, H. O., J. McCaffrey, C. M. McCrudden, A. Zholobenko, A. A. Ali, J. W. McBride, A. S. Massey, S. Pentlavalli, K. H. Chen, G. Cole, S. P. Loughran, N. J. Dunne, R. F. Donnelly, V. L. Kett, and T. Robson. 2014. 'Development and characterization of self-assembling nanoparticles using a bio-inspired amphipathic peptide for gene delivery', *J Control Release*, 189: 141-9.

McCrudden, C. M., J. W. McBride, J. McCaffrey, E. M. McErlean, N. J. Dunne, V. L. Kett, J. A. Coulter, T. Robson, and H. O. McCarthy. 2018. 'Gene therapy with RALA/iNOS composite nanoparticles significantly enhances survival in a model of metastatic prostate cancer', *Cancer Nanotechnol*, 9: 5.

McCrudden, Cian M., John W. McBride, Joanne McCaffrey, Ahlam A. Ali, Nicholas J. Dunne, Vicky L. Kett, Jonathan A. Coulter, Tracy Robson, and Helen O. McCarthy. 2017. 'Systemic RALA/iNOS Nanoparticles: A Potent Gene Therapy for Metastatic Breast Cancer Coupled as a Biomarker of Treatment', *Molecular Therapy - Nucleic Acids*, 6: 249-58.

Medina-Alarcon, K. P., A. R. Voltan, B. Fonseca-Santos, I. J. Moro, F. de Oliveira Souza, M. Chorilli, C. P. Soares, A. G. Dos Santos, M. J. S. Mendes-Giannini, and A. M. Fusco-Almeida. 2017. 'Highlights in nanocarriers for the treatment against cervical cancer', *Mater Sci Eng C Mater Biol Appl*, 80: 748-59.

Mohsen, M. Mady. 2011. 'Interaction of DNA and polyethylenimine: Fourier-transform infrared (FTIR) and differential scanning calorimetry (DSC) studies', *International Journal of the Physical Sciences*, 6.

Pahle, J., and W. Walther. 2016. 'Vectors and strategies for nonviral cancer gene therapy', *Expert Opin Biol Ther*, 16: 443-61.

Petit, Tristan, and Ljiljana Puskar. 2018. 'FTIR spectroscopy of nanodiamonds: Methods and interpretation', *Diamond and Related Materials*, 89: 52-66.

Pezzoli, D., E. Giupponi, D. Mantovani, and G. Candiani. 2017. 'Size matters for in vitro gene delivery: investigating the relationships among complexation protocol, transfection medium, size and sedimentation', *Sci Rep*, 7: 44134.

Pfeffer, C. M., and A. T. K. Singh. 2018. 'Apoptosis: A Target for Anticancer Therapy', *Int J Mol Sci*, 19.

Rizzo, A. E., and S. Feldman. 2018. 'Update on primary HPV screening for cervical cancer prevention', *Curr Probl Cancer*, 42: 507-20.

Sambrook, J., E. F. Fritsch, and T. Maniatis. 1989. *Molecular cloning: a laboratory manual* (Cold Spring Harbor Laboratory Press: Cold Spring Harbor, NY).

Santos, J., F. Sousa, J. Queiroz, and D. Costa. 2014. 'Rhodamine based plasmid DNA nanoparticles for mitochondrial gene therapy', *Colloids Surf B Biointerfaces*, 121: 129-40.

Scheffner, Martin, Jon M. Huibregtse, Richard D. Vierstra, and Peter M. Howley. 1993. 'The HPV-16 E6 and E6-AP complex functions as a ubiquitin-protein ligase in the ubiquitination of p53', *Cell*, 75: 495-505.

Shao, D., H. Wu, F. Shen, H. Wu, and J. Quan. 2017. 'Carbon dioxide-modified polyethylenimine as a novel gene delivery vector and its in vitro validation', *J Biomater Appl*, 31: 1257-66.

Sharma, B., W. Ma, I. M. Adjei, J. Panyam, S. Dimitrijevic, and V. Labhasetwar. 2011. 'Nanoparticle-mediated p53 gene therapy for tumor inhibition', *Drug Deliv Transl Res*, 1: 43-52.

Silva, S., A. J. Almeida, and N. Vale. 2019. 'Combination of Cell-Penetrating Peptides with Nanoparticles for Therapeutic Application: A Review', *Biomolecules*, 9.

Singha, Tapan Kumar, Pooja Gulati, Aparajita Mohanty, Yogender Pal Khasa, Rajeev Kumar Kapoor, and Sanjay Kumar. 2017. 'Efficient genetic approaches for improvement of plasmid based expression of recombinant protein in Escherichia coli : A review', *Process Biochemistry*, 55: 17-31.

Teo, P. Y., W. Cheng, J. L. Hedrick, and Y. Y. Yang. 2016. 'Co-delivery of drugs and plasmid DNA for cancer therapy', *Adv Drug Deliv Rev*, 98: 41-63.

Thomas, Miranda, David Pim, and Lawrence Banks. 1999. 'The role of the E6-p53 interaction in the molecular pathogenesis of HPV', *Oncogene*, 18: 7690-700.

Udhayakumar, V. K., A. De Beuckelaer, J. McCaffrey, C. M. McCrudden, J. L. Kirschman, D. Vanover, L. Van Hoecke, K. Roose, K. Deswarte, B. G. De Geest, S. Lienenklaus, P. J. Santangelo, J. Grooten, H. O. McCarthy, and S. De Koker. 2017. 'Arginine-Rich Peptide-Based mRNA Nanocomplexes Efficiently Instigate Cytotoxic T Cell Immunity Dependent on the Amphipathic Organization of the Peptide', *Adv Healthc Mater*, 6.

Valente, J. F. A., A. Sousa, V. M. Gaspar, J. A. Queiroz, and F. Sousa. 2018. 'The biological performance of purified supercoiled p53 plasmid DNA in different cancer cell lines', *Process Biochemistry*, 75: 240-49.

Valente, J. F., A. Sousa, J. A. Queiroz, and F. Sousa. 2014. 'Selective purification of supercoiled p53-encoding pDNA with L-methionine-agarose matrix', *Anal Biochem*, 459: 61-9.

Venere, Monica, Kuntal De, Ji Young Yoo, and Balveen Kaur. 2018. 'Apoptosis Pathways and Chemotherapy in Brain Tumors.' in, *Handbook of Brain Tumor Chemotherapy, Molecular Therapeutics, and Immunotherapy*.

Vu, M., J. Yu, O. A. Awolude, and L. Chuang. 2018. 'Cervical cancer worldwide', *Curr Probl Cancer*, 42: 457-65.

Wang, J., B. Dou, and Y. Bao. 2014. 'Efficient targeted pDNA/siRNA delivery with folate-low-molecular-weight polyethyleneimine-modified pullulan as non-viral carrier', *Mater Sci Eng C Mater Biol Appl*, 34: 98-109.

Wyman, T. B., F. Nicol, O. Zelphati, P. V. Scaria, C. Plank, and F. C. Szoka, Jr. 1997. 'Design, synthesis, and characterization of a cationic peptide that binds to nucleic acids and permeabilizes bilayers', *Biochemistry*, 36: 3008-17.

Zhang, Bingyang, Hu Zhang, Sheng Dai, and Jingxiu Bi. 2017. 'Cell-penetrating peptide-labelled smart polymers for enhanced gene delivery', *Engineering in Life Sciences*, 17: 193-203.

Chapter VII – Annexes

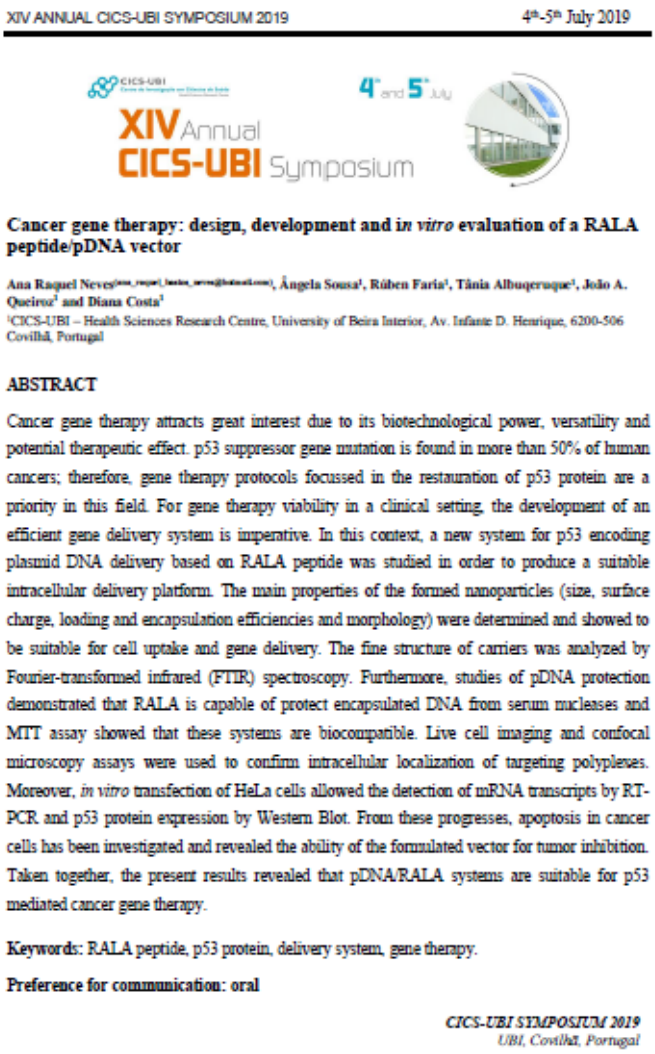

XIV ANNUAL CICS-UBI SYMPOSIUM 2019 4th-5th July 2019

XIV Annual CICS-UBI Symposium

4th and 5th July

Cancer gene therapy: design, development and *in vitro* evaluation of a RALA peptide/pDNA vector

Ana Raquel Neves[1], Ângela Sousa[1], Rúben Faria[1], Tânia Albuquerque[1], João A. Queiroz[1] and Diana Costa[1]

[1]CICS-UBI – Health Sciences Research Centre, University of Beira Interior, Av. Infante D. Henrique, 6200-506 Covilhã, Portugal

ABSTRACT

Cancer gene therapy attracts great interest due to its biotechnological power, versatility and potential therapeutic effect. p53 suppressor gene mutation is found in more than 50% of human cancers; therefore, gene therapy protocols focussed in the restauration of p53 protein are a priority in this field. For gene therapy viability in a clinical setting, the development of an efficient gene delivery system is imperative. In this context, a new system for p53 encoding plasmid DNA delivery based on RALA peptide was studied in order to produce a suitable intracellular delivery platform. The main properties of the formed nanoparticles (size, surface charge, loading and encapsulation efficiencies and morphology) were determined and showed to be suitable for cell uptake and gene delivery. The fine structure of carriers was analyzed by Fourier-transformed infrared (FTIR) spectroscopy. Furthermore, studies of pDNA protection demonstrated that RALA is capable of protect encapsulated DNA from serum nucleases and MTT assay showed that these systems are biocompatible. Live cell imaging and confocal microscopy assays were used to confirm intracellular localization of targeting polyplexes. Moreover, *in vitro* transfection of HeLa cells allowed the detection of mRNA transcripts by RT-PCR and p53 protein expression by Western Blot. From these progresses, apoptosis in cancer cells has been investigated and revealed the ability of the formulated vector for tumor inhibition. Taken together, the present results revealed that pDNA/RALA systems are suitable for p53 mediated cancer gene therapy.

Keywords: RALA peptide, p53 protein, delivery system, gene therapy.

Preference for communication: oral

CICS-UBI SYMPOSIUM 2019
UBI, Covilhã, Portugal

Figure 34: Abstract submitted to XIV Annual CICS-UBI Symposium.

Journal: ACS Applied Materials & Interfaces
Manuscript ID: am-2019-10754y
Title: "Cancer gene therapy mediated by RALA/plasmid DNA vectors: Nitrogen to Phosphate groups ratio (N/P) as a tool for tunable transfection efficiency and apoptosis"
Authors: Neves, Ana; Sousa, Angela; Faria, Rúben; Albuquerque, Tânia; Queiroz, João; Costa, Diana
Manuscript Status: Submitted

Dear Dr. Costa:

Your manuscript has been successfully submitted to ACS Applied Materials & Interfaces.

Please reference the above manuscript ID in all future correspondence or when calling the office for questions. If there are any changes in your contact information, please log in to ACS Paragon Plus with your ACS ID at http://paragonplus.acs.org/login and select "Edit Your Profile" to update that information.

You can view the status of your manuscript by checking your "Authoring Activity" tab on ACS Paragon Plus after logging in to http://paragonplus.acs.org/login.

Figure 35: Scientific article submission proof email.